CONFIDENTIAL

N 62 64198 04

Copy
RM E56L19

NACA RM E56L19

NACA

CASE FILE
COPY

RESEARCH MEMORANDUM

PERFORMANCE OF EXTERNAL-COMPRESSION BUMP INLET AT MACH NUMBERS OF 1.5 TO 2.0

By Paul C. Simon, Dennis W. Brown, and Ronald G. Huff

Lewis Flight Propulsion Laboratory
Cleveland, Ohio

CLASSIFICATION CHANGED TO UNCLASSIFIED
AUTHORITY: NASA TECHNICAL PUBLICATIONS ANNOUNCEMENTS NO. 2
EFFECTIVE DATE: AUGUST 19, 1960 WHL

CLASSIFIED DOCUMENT

This material contains information affecting the National Defense of the United States within the meaning of the espionage laws, Title 18, U.S.C., Secs. 793 and 794, the transmission or revelation of which in any manner to an unauthorized person is prohibited by law.

NATIONAL ADVISORY COMMITTEE
FOR AERONAUTICS

WASHINGTON

April 24, 1957

CONFIDENTIAL

NATIONAL ADVISORY COMMITTEE FOR AERONAUTICS

RESEARCH MEMORANDUM

PERFORMANCE OF EXTERNAL-COMPRESSION BUMP INLET AT MACH NUMBERS OF 1.5 TO 2.0

By Paul C. Simon, Dennis W. Brown, and Ronald G. Huff

4350 CU-1

SUMMARY

An experimental investigation of a one-fifth-scale model of the forebody of a proposed supersonic fighter was conducted to determine the internal performance and configuration drag of various twin-side inlets. Inlets of the external-compression ramp and bump types, having various types and combinations of boundary-layer bleed, were tested. All configurations had internal contraction sufficient to prevent supersonic starting at the Mach numbers investigated. The configurations were tested at Mach numbers of 1.5, 1.8, and 2.0; angles of attack from 0° to 10°; and angles of yaw from 0° to 5°.

The performance of the external-compression bump inlet was superior to that of the ramp inlet at all flight conditions investigated. The performance of the bump inlet at critical mass-flow conditions was generally insensitive to variations in angle of attack and yaw. Adequate inlet stability range and suitable sensor pressures for a bypass control were observed at all flight conditions.

INTRODUCTION

An experimental investigation of a one-fifth-scale model of the forebody of a proposed supersonic fighter was conducted in the 8- by 6-foot supersonic wind tunnel of the NACA Lewis laboratory for the purpose of evaluating several twin-side-inlet air induction systems. The evaluation was made on the basis of configuration axial force, inlet mass flow, pressure recovery, stability, and compressor-inlet total-pressure distortions. Subsonic-diffuser pressure ratios were recorded for possible use as input signals to a diffuser bypass control system. Performance was evaluated for a range of free-stream Mach numbers, mass-flow ratios, and angles of attack and yaw.

External-compression bump and ramp inlets were tested with various amounts of compression surface and inlet throat boundary-layer bleed. In addition, configuration performance for both a conical and a flat canopy windshield was determined.

The Reynolds number per foot, based on free-stream conditions, varied between 4 and 5 million.

SYMBOLS

A	area, sq ft
A_B	fuselage forebody base area, 0.8605 sq ft
$(A/A_3)_d$	ratio of total diffuser flow area of twin inlets to compressor-inlet flow area
C_F	configuration external-axial-force coefficient, $\frac{F}{q_0 A_B}$
F	configuration external axial force, lb (positive downstream)
M	Mach number
m	mass flow, ρVA
m/m_0	mass-flow ratio, $\frac{m}{\rho_0 V_0 A_t}$
P	total pressure, lb/sq ft
P_3/P_0	compressor-inlet total-pressure ratio
$\bar{P}_3/P_0$	compressor-inlet total-pressure recovery (average across duct)
$\Delta P_3/\bar{P}_3$	total-pressure distortion at compressor inlet
p	static pressure, lb/sq ft
$(p_1/P_1)_r$	pressure ratio in right-hand diffuser at station 1
p_2/P_2	pressure ratio at diffuser station 2
p_3/P_0	compressor-inlet static-pressure ratio
$\Delta p_3/P_0$	inlet stability pressure amplitude at compressor inlet
q	dynamic pressure, $\frac{\gamma}{2}(pM^2)$, lb/sq ft
T	total temperature, $^\circ R$
V	velocity, ft/sec

w	weight flow, lb/sec
$\frac{w_i\sqrt{\theta}}{\delta_3 A_3}$	inlet weight flow per unit area referenced to compressor inlet and standard sea-level conditions, lb/(sec)(sq ft)
α	fuselage angle of attack, deg
γ	ratio of specific heats
δ	ratio of total pressure to NACA standard sea-level pressure, P/2116.2
θ	ratio of total temperature to NACA standard sea-level temperature, T/518.7
ρ	mass density, slugs/cu ft
ψ	fuselage angle of yaw, deg

Subscripts:

b	inlet boundary-layer bleed
bp	diffuser bypass
i	inlet duct
t	inlet throat
0	free-stream conditions
1	diffuser station 1 (model station 37.10 in.)
2	diffuser station 2 (model station 59.25 in.)
3	compressor inlet (model station 66.83 in.)

APPARATUS AND PROCEDURE

The model was a one-fifth-scale forebody of a proposed supersonic airplane having twin side inlets designed to supply air to one turbojet engine. A photograph of the model mounted on the sting support system in the tunnel is presented in figure 1, and a general assembly drawing of the model is given in figure 2. The airflow through the diffuser system was varied by means of a remotely controlled conical plug at the diffuser-discharge duct exit, and the axial forces were measured by an internal strain-gage balance. Model angles of attack and yaw were varied by remote operation of the support strut.

4350
CU-1 back

Inlets

Two types of external-compression inlets were investigated, a bump inlet and a ramp inlet. Both inlets were designed at a free-stream Mach number of 1.6 to compress the nonuniform flow, created by the fuselage nose and the pilot's canopy, in such a manner as to generate a uniform Mach number of 1.4 at the face of the inlets.

The bump inlet utilized a contoured hump located in front of each inlet. Details of the bump inlet are shown in figure 3(a). Boundary-layer bleed systems, consisting of perforations on the bump surface and perforations and/or a flush slot on the inlet floor, were incorporated on the bump inlet to remove that portion of the boundary-layer air that entered the inlet. The bleed surface was arbitrarily divided into five areas, as illustrated in figure 3(b). All air bled through the perforated areas or slot entered a bleed chamber (fig. 3(b)), directly under the bleed surfaces, and was discharged through two exits located on either side of the inlet cowl. Various combinations of bleed areas as enumerated in table I were tested. In one combination, air bled from the forward perforated area was discharged out the bleed-chamber exits through two independent 5/8-inch-inside-diameter tubes. This was done to prevent the high bleed-chamber pressure, originating at the throat slot, from forcing air out the perforations of the forward area. No attempt was made to measure the bleed weight flow.

The ramp inlet was essentially a two-dimensional wedge-type compression surface (fig. 3(c)). However, the leading edge of the ramp was curved so as to be equidistant from the fuselage surface. The ramp inlet was tested with and without a throat bleed slot, as noted in table I. A fuselage boundary-layer diverter was installed beneath the ramp (fig. 3(c)).

Diffuser

The diffuser flow-area variations of both the bump and ramp inlets are given in figure 4. Both the bump and ramp diffusers had internal contraction exceeding the maximum theoretical for starting at the free-stream Mach numbers tested. The equivalent cone angle of the diffuser, from the throat to the maximum area, was 1.77° for the bump diffuser and 1.74° for the ramp diffuser.

Bypass

The diffuser bypass on the full-scale operational airplane is designed to permit the inlet to operate at optimum net propulsive thrust, to make possible turbojet-engine operation without inlet instability,

4350

and, in addition, to supply the secondary-flow requirements of an ejector nozzle. These requirements demand a variable bypass. The model bypass, although a scaled version of the operational bypass, was not variable and was fixed at the minimum open position for the data reported herein. The nearly flush opening of the bypass (see fig. 2) was annular in shape and was located circumferentially around the diffuser just upstream of the compressor-inlet station. A small diffuser boundary-layer scoop was incorporated in the bypass ring. Thus low-energy air was scooped off and ducted, along with the bypass air, downstream to a discharge at the model base. The ratio of boundary-layer scoop area plus bypass area to compressor-inlet flow area A_{bp}/A_3 was 0.066.

Canopy

The two types of canopies tested, the flat and the conical windshields, and their locations relative to the bump inlet are illustrated in the isometric views shown in figure 5.

Instrumentation and Data Reduction

Pressure orifices and pitot tubes associated with the model were located in the internal region of the diffuser system and the fuselage base. Compressor-inlet total pressure $\overline{P}_3$ was determined by averaging the measured total pressures at the compressor inlet, station 3 (model station 66.83 in.), where the pitot tubes were located at the centroids of equal areas (fig. 5). The compressor-inlet total-pressure distortions $\Delta P_3/\overline{P}_3$ were also evaluated from these tubes. Total-pressure distortion was defined as the maximum indicated total pressure minus the minimum total pressure divided by $\overline{P}_3$, the average of all the tubes. The pitot tubes closest to the diffuser wall were 4.6 percent of the diffuser diameter from the wall surface.

The compressor-inlet mass flow m_3 was determined from the average of four static-pressure orifices at model station 87.83 inches (3.46 compressor-inlet diam downstream of compressor-inlet station) and the known area ratio between that station and the throat formed by the remotely controlled exit plug, where the flow was assumed to be choked. The bypass mass flow m_{bp} was evaluated from the static and total pressures measured at a station of known area in the bypass duct. The inlet mass flow m_i is simply the sum of the compressor-inlet and bypass flows.

The axial forces presented represent only external pressure and friction forces; the base force and the change in total momentum of the internal flow from the free stream to the duct discharge have been excluded from the model forces.

The total amplitude of the compressor-inlet static-pressure fluctuations (buzz) was determined by a dynamic-pressure pickup located near the compressor-inlet station.

The model was rolled 84° clockwise to position the left inlet in line with the schlieren system, and the performance of the inlet in yaw was obtained during this rolled condition. The 84° roll position produced 20- and 35-minute angles of attack at 2°52' and 4°47' angles of yaw, respectively.

In order to obtain controls data, configuration B(2,3)F was modified by the addition of pressure-sensing instrumentation designed to supply input signals to a diffuser bypass control. Two independent sets of pressure pickups were installed, diffuser stations 1 and 2, to provide a choice between two possible locations. Both sets of instrumentation were of the Mach number control type described in reference 1. A rake consisting of five pitot tubes and one static orifice was installed near the throat (station 1) of each diffuser duct. The controls instrumentation installed at diffuser station 2 (fig. 6) consisted of four static-pressure orifices and a total-pressure rake mounted laterally across the diffusers just upstream of where the twin ducts join into one. The average pressure of this rake was approximately equal to the pressure obtainable from a slotted orifice described in reference 1. (A rake was used because it offered less area blockage in the model.) Thus, the resulting pressure ratio p_2/P_2 could possibly be used as a Mach number control parameter.

4350

RESULTS AND DISCUSSION

Performance Charts

Performance of configurations. - The performance plots of the external-compression bump and ramp inlets with various boundary-layer bleed systems are presented in figure 7. On each plot the three performance parameters, compressor-inlet total-pressure recovery, compressor-inlet total-pressure distortion, and external axial-force coefficient, are plotted as a function of the compressor-inlet mass-flow ratio for two angles of attack and free-stream Mach numbers of 1.5 and 1.8. The region of unstable inlet operation, where the maximum total amplitude of the static-pressure fluctuations at the compressor inlet is greater than 5 percent of the free-stream total pressure, is shown by dashed curves. Superimposed on each set of total-pressure recovery curves is a grid of corrected weight-flow lines.

All configurations had about the same pressure recovery and a wide range of buzz-free match points for turbojet-engine operation, as shown in figure 7. Configuration B(2,3)F was selected for a more detailed

study because it had the least amount of bleed surface area and therefore should also have the smallest drag due to bleed. The performance of configuration B(2,3)F is presented in figures 8(a) and (b) for Mach numbers up to 2.0, angles of attack up to 9°37', and angles of yaw up to 5°. It can be noted that the important performance variables at critical mass-flow ratio are relatively insensitive to variations in angle of attack and yaw. The performance of the bump-inlet configuration with a conical windshield can be compared with that of the flat windshield in figures 8(c), (d), and (e).

4350

Performance summary charts. - The performance of configurations B(2,3), R(0)F, and R(5)F during critical mass-flow conditions is summarized in figure 9. At this mass-flow condition, the performance of the bump inlet was superior to that of the ramp inlets (fig. 9(a)). For example, the bump-inlet recovery was about 2 percent greater than that of configuration R(0)F, the distortion was about 18 percent less, and the drag about 7 percent less at Mach numbers of 1.5 and 1.8.

The effect of angle of attack on the critical inlet performance of configuration B(2,3)F is presented in figure 9(b) for the Mach number range investigated. As can be noted from the figure, the important performance variables were insensitive to angle of attack up to 10°.

The effect of modifying the cockpit canopy from a flat windshield to a conical windshield (fig. 5) for angles of attack of 0°, 5°, and 9°37' is presented in figure 9(c). The modification produced an improvement in both critical pressure recovery and axial-force coefficient at all Mach numbers and angles of attack investigated. The greatest gains were at a Mach number of 1.8, where C_F decreased about 10 percent at $\alpha = 5°$ and $\overline{P}_3/P_0$ increased approximately 2 percent at $\alpha = 9°37'$.

Flow Characteristics

Mass flow. - The compressor-inlet mass flow and the concomitant bypass mass flow for configuration B(2,3)F is presented in figure 10 at all conditions tested. The bypass mass flow is the sum of the boundary-layer scoop mass flow and the mass flow which passed through the bypass opening (0.037 in.). A slight difference in bypass mass flow exists between the angle-of-attack and the angle-of-yaw conditions because for the angle-of-attack condition the bypass was inadvertantly unchoked, thereby reducing m_{bp}. The flow coefficient (measured bypass mass flow divided by theoretical bypass mass flow assuming $\overline{P}_3$ at the choked areas) for the bypass flush slot plus diffuser boundary-layer scoop was estimated to be 0.9 (approximately).

Schlieren photographs. - Figure 11 presents a group of typical schlieren photographs of the inlet shock structure of configuration B(2,3)F at zero angle of attack. For each free-stream and attitude condition, three photographs at different inlet mass-flow ratios are shown, one of the inlet at critical operation and two having subcritical mass flows. No schlieren photographs were taken at angles of attack other than zero degree.

Total-pressure contours. - Typical compressor-inlet total-pressure contours for conditions at or near critical mass flow are presented in figure 12 for configurations B(2,3)F, R(0)F, and R(5)F at various Mach numbers and angles of attack and yaw.

Inlet stability. - Inlet stability characteristics for configuration B(2,3)F are presented in figure 13 for Mach numbers of 1.5, 1.8, and 2.0 and angles of attack of 0°, 5°, and $9^\circ 37'$. The variation of the maximum amplitude of the compressor-inlet static-pressure fluctuations $\Delta p_3/P_0$ with changes in inlet corrected weight flow $w_i\sqrt{\theta}/\delta_3 A_3$ is presented to indicate the rate at which the inlet proceeds into buzz.

Controls. - To aid in determining a suitable diffuser Mach number type of bypass control, both stations 1 and 2 were instrumented with static- and total-pressure sensors. The objective of the measurements at station 1 was to determine if the pressure ratio p_1/P_1 at one location would show a consistent variation with changes in inlet mass-flow ratio m_i/m_0 and would be relatively insensitive to variations in angle of pitch and yaw. The static- to total-pressure ratio at station 1 for the five pitot tubes of the right diffuser are shown in figure 14(a) as a function of $w_i\sqrt{\theta}/\delta_3 A_3$. No left-diffuser data or yaw data are presented because the static-pressure measurement in the left duct was in error. For a typical turbojet engine, an estimate of the net propulsive thrust variation with $w_i\sqrt{\theta}/\delta_3 A_3$ (not presented) indicated that the maximum value occurred at 41 and 39 pounds per second per square foot for free-stream Mach numbers of 1.5 and 1.8, respectively. It can be noted that the bypass control pressure ratio p_1/P_1 for all tubes except number 1 could be scheduled for a value of 0.665 and 0.705 at Mach numbers of 1.5 and 1.8, respectively, for optimum performance at angles of attack up to 10°.

The controls pressure ratios at diffuser station 2 are presented in figure 14(b) for configuration B(2,3)F at Mach numbers of 1.5 and 1.8 and the angles of attack and yaw tested. This average static- to total-pressure ratio indicates that it also would make a suitable bypass control parameter because of its insensitivity to variations in angle of attack or yaw.

SUMMARY OF RESULTS

A supersonic wind-tunnel investigation of a one-fifth-scale model of the forebody of a proposed fighter airplane was conducted to determine the internal performance and configuration drag of various twin side inlets for a range of Mach numbers and angles of attack and yaw. A summary of the more important findings is as follows:

1. The performance of the external-compression bump inlet was superior to that of the external-compression ramp inlet.

2. The stability of all inlets investigated was sufficient to provide a wide range of buzz-free subcritical match points for turbojet operation.

3. The critical performance of the bump inlet was generally insensitive to angles of attack to 10° and angles of yaw to 5°.

4. A modification of the cockpit canopy, from a flat windshield to a conical windshield, produced improvements in both pressure recovery and configuration drag.

5. Measured values of static- to total-pressure ratio near the subsonic-diffuser discharge were indicated to be adequate for input to a bypass control. Averaged values proved insensitive to variations in both angle of attack and yaw.

Lewis Flight Propulsion Laboratory
National Advisory Committee for Aeronautics
Cleveland, Ohio, December 20, 1956

REFERENCE

1. Whalen, Paul P., and Wilcox, Fred A.: Use of Subsonic Diffuser Mach Number as a Supersonic-Inlet Control Parameter. NACA RM E56F05, 1956.

4350

TABLE I. - LIST OF CONFIGURATIONS INVESTIGATED

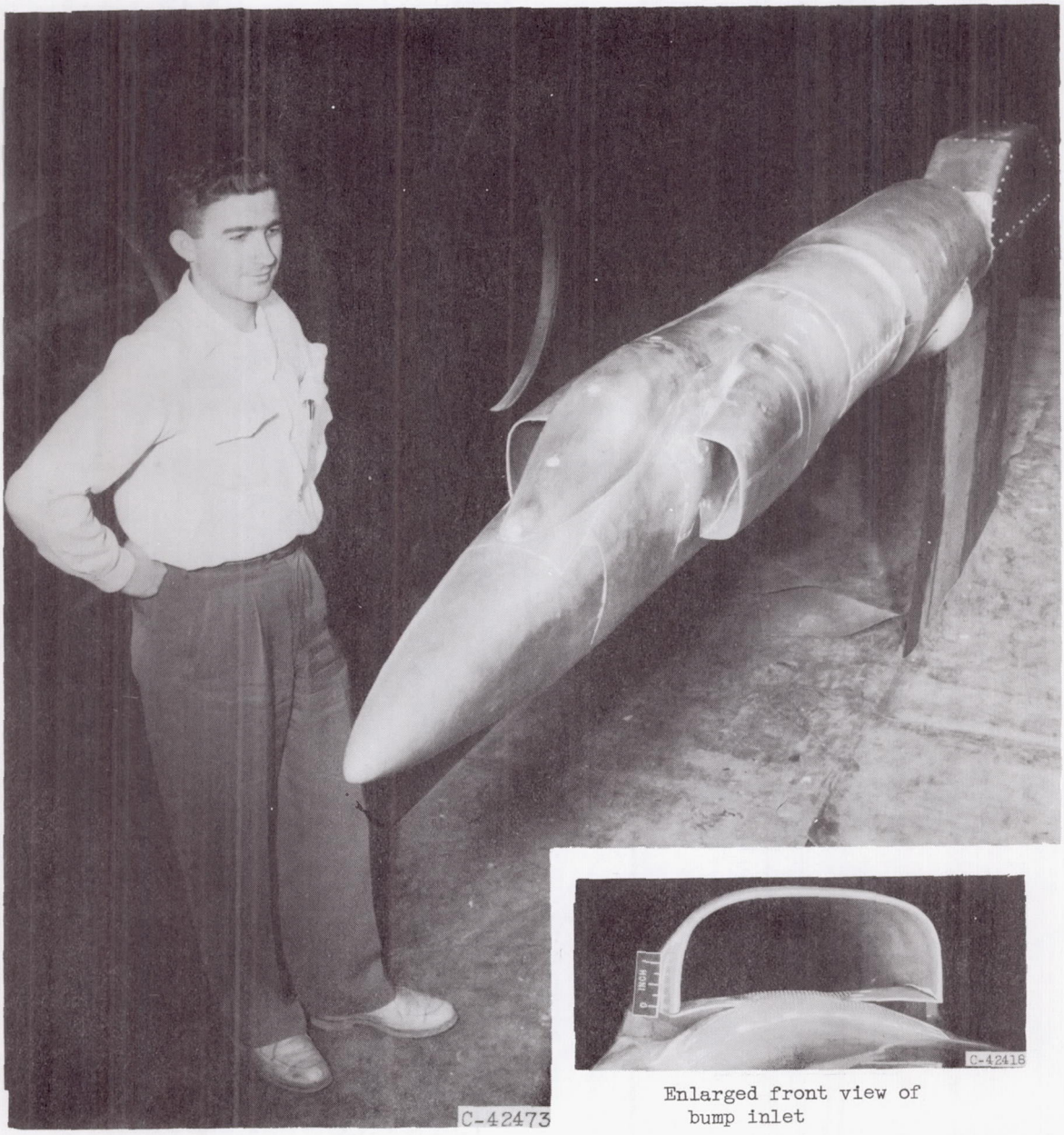
Configuration nomenclature	Total bleed-area ratio, A_b/A_t	Perforated area per unit surface area (hole diam. = 0.070 in.), percent	Flush-slot width, in. (area 5)
B(2,3)F[a]	0.195	25	---
B(2,3)C	.195	25	---
B(1,2,3)F	.319	25	---
B(2,3,5)F	.385	25	3/8
B(1,5)FV[b]	.415	25	5/8
B(2,3,4,5)F	.557	25	3/8
R(0)F	0	0	---
R(5)F	.286	0	5/8

B	External-compression bump inlet (fig. 3(a))
C	Conical windshield (fig. 5)
F	Flat windshield (fig. 5)
R	External-compression ramp inlet (fig. 3(c))
0	No boundary-layer bleed (fig. 3(c))
1,2,3,4	Perforated areas for boundary-layer bleed (fig. 3(b))
5	Flush slot at diffuser throat for boundary-layer bleed (figs. 3(b) and (c))

[a]Selected for a more extensive study.

[b]This configuration was tested with the bleed air from area 1 discharged through an independent vent.

4350
CU-2 back



Enlarged front view of bump inlet

Figure 1. - Photograph of model installed in 8- by 6-foot supersonic wind tunnel.

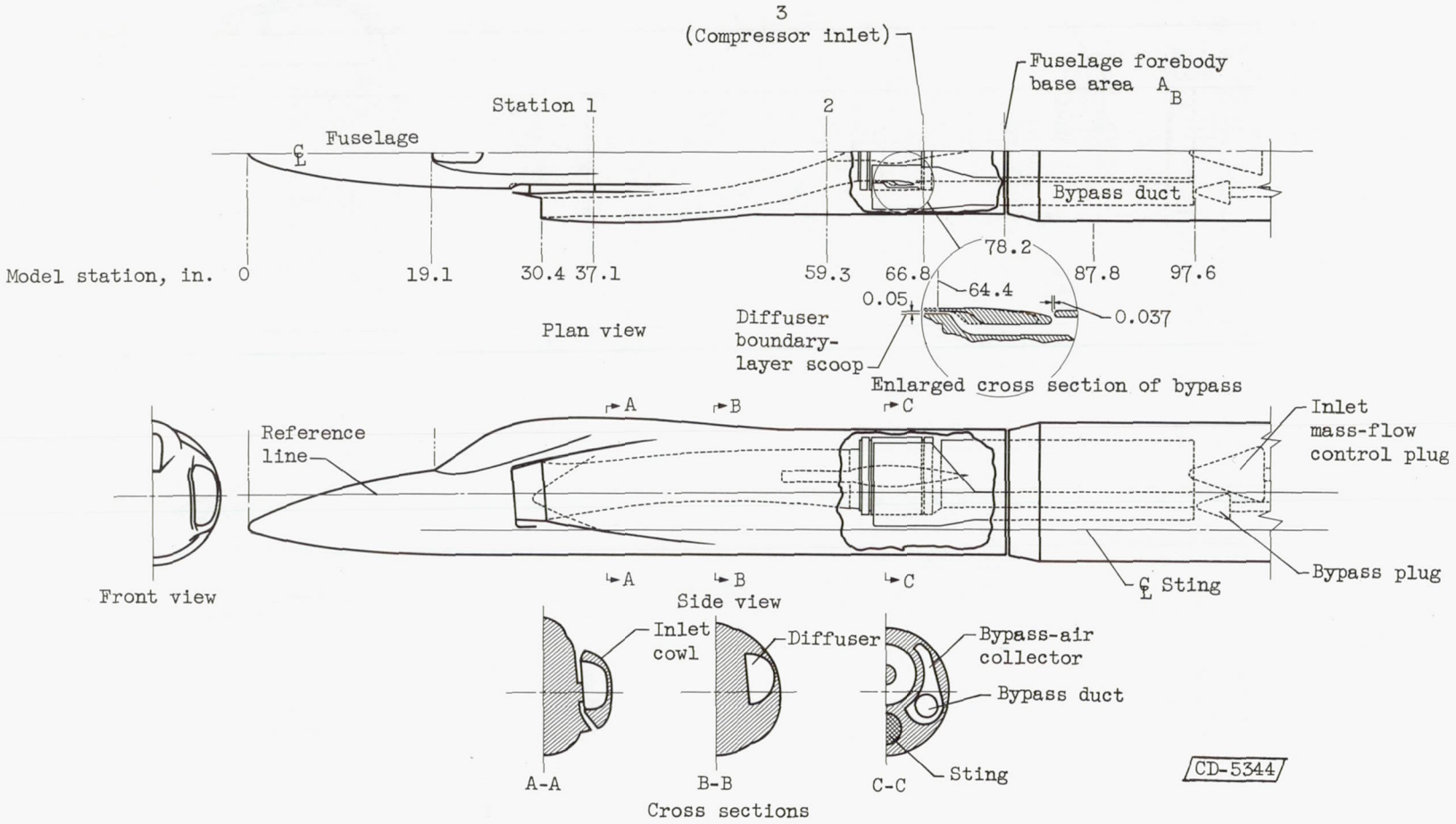
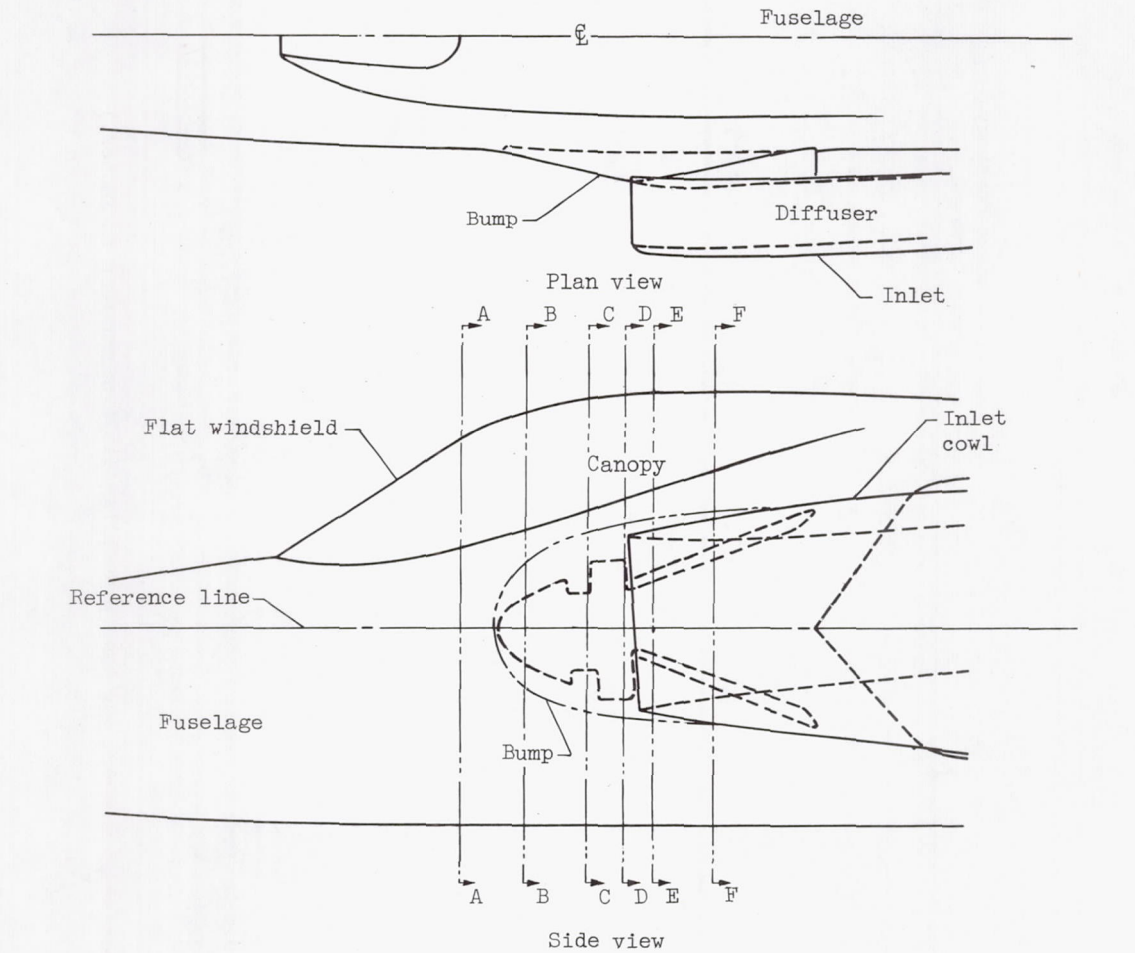
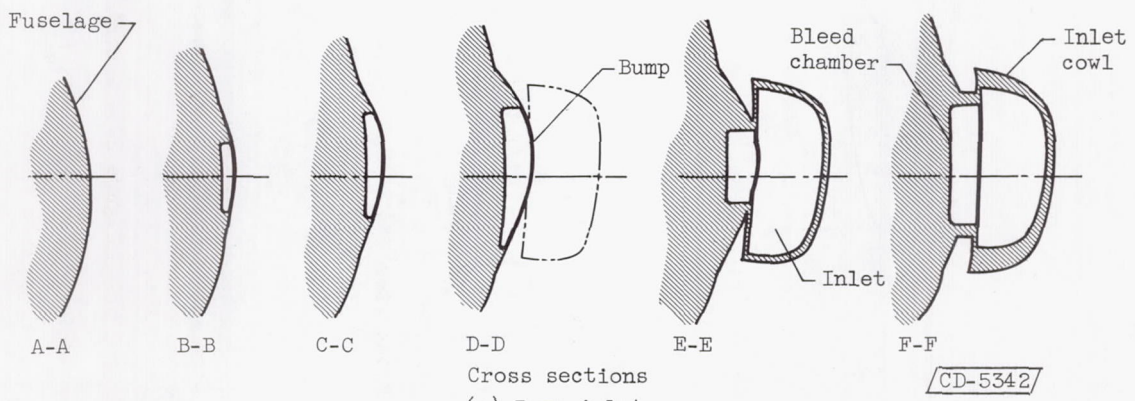


Figure 2. - General assembly of model and bypass details. (All dimensions in inches.)

4350

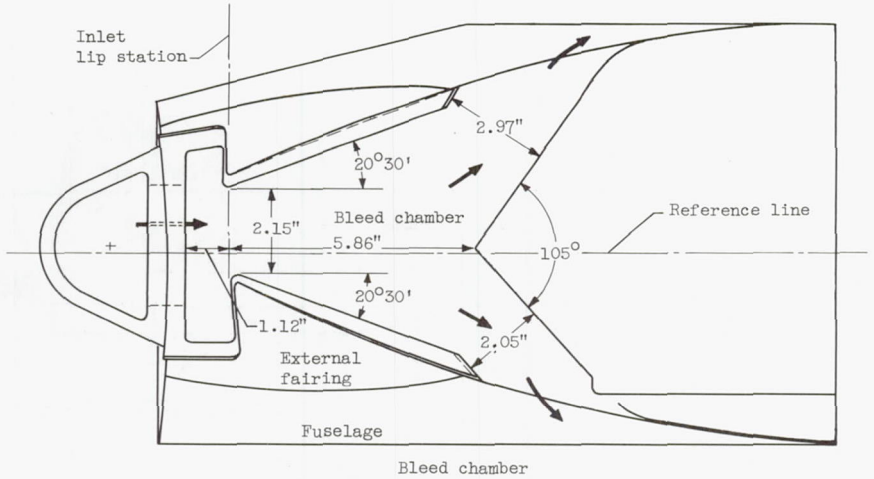




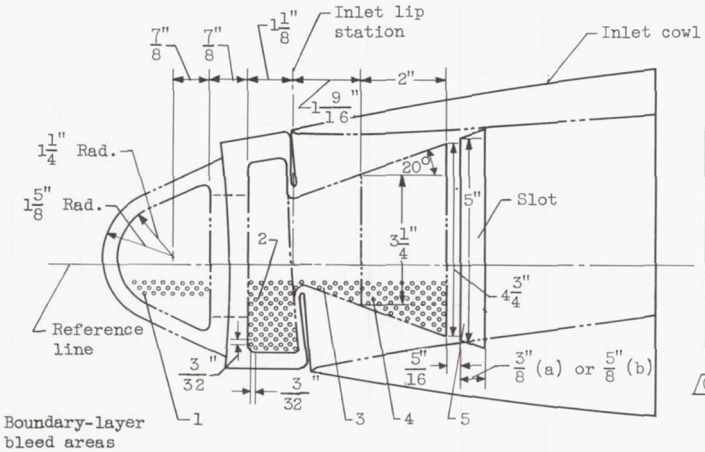
Cross sections

(a) Bump inlet.

Figure 3. - Inlets.

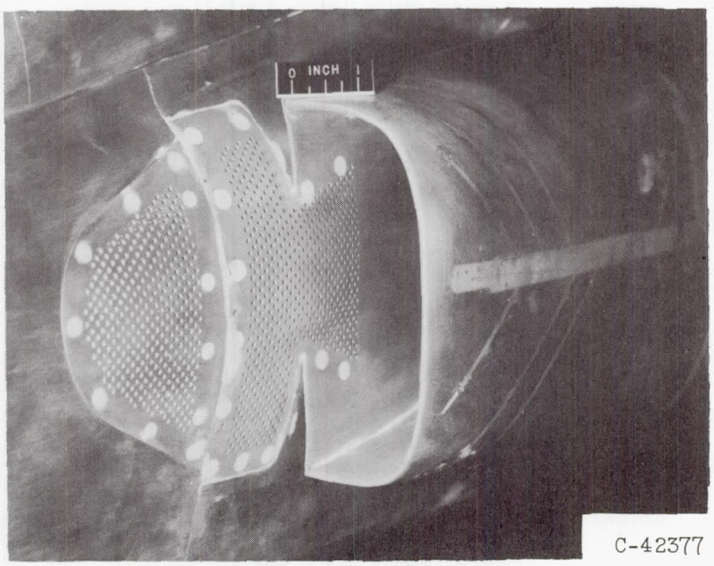


Bleed chamber



Boundary-layer bleed	
Area	Open area, sq in.
1	1.33
2	1.21
3	.88
4	1.84
5a	2.05
5b	3.13

CD-5318

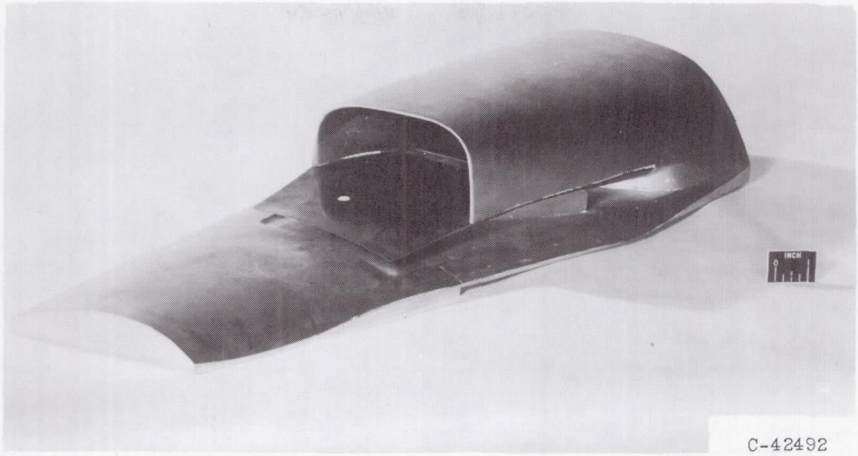


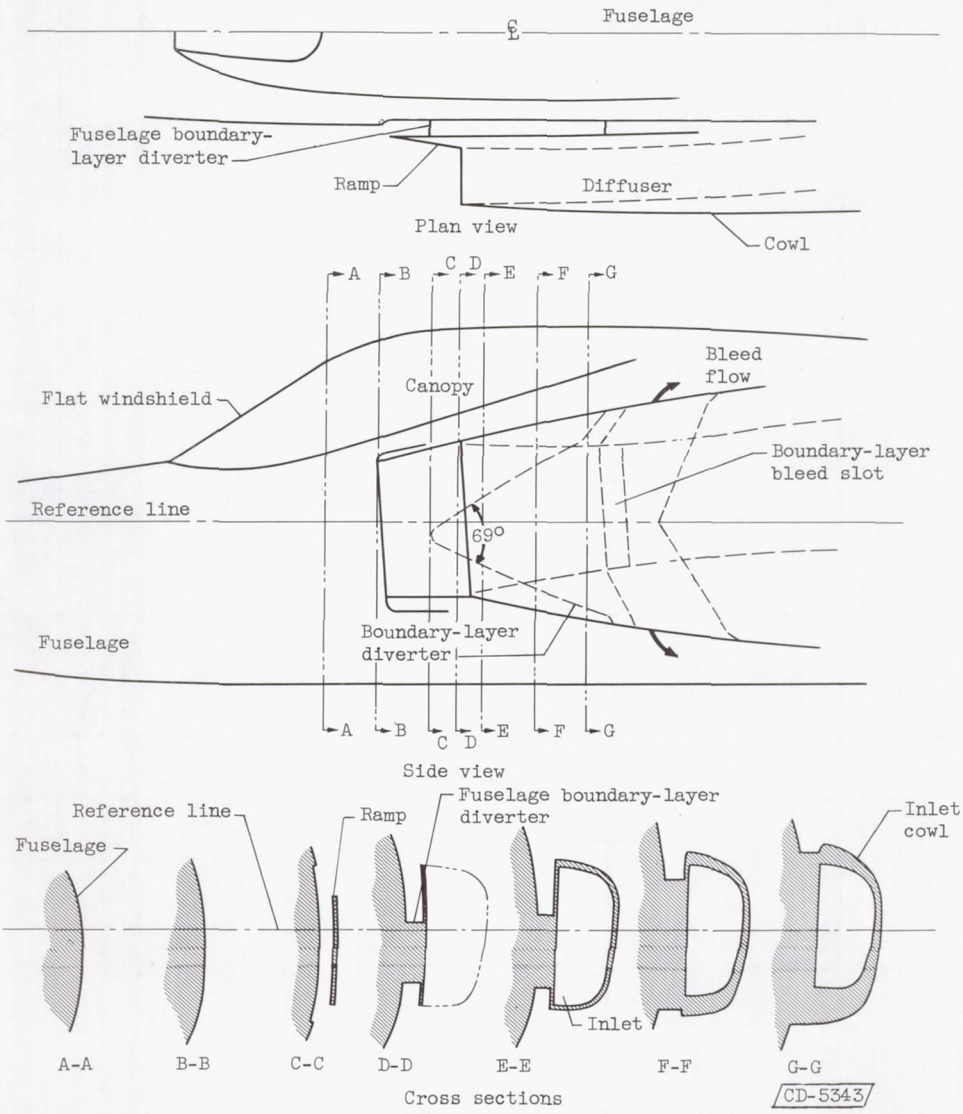
Perforated areas 1, 2, and 3

(b) Bump-inlet bleed surface and bleed chamber.

Figure 3. - Continued. Inlets.

4350





(c) Ramp inlet.

Figure 3. - Concluded. Inlets.

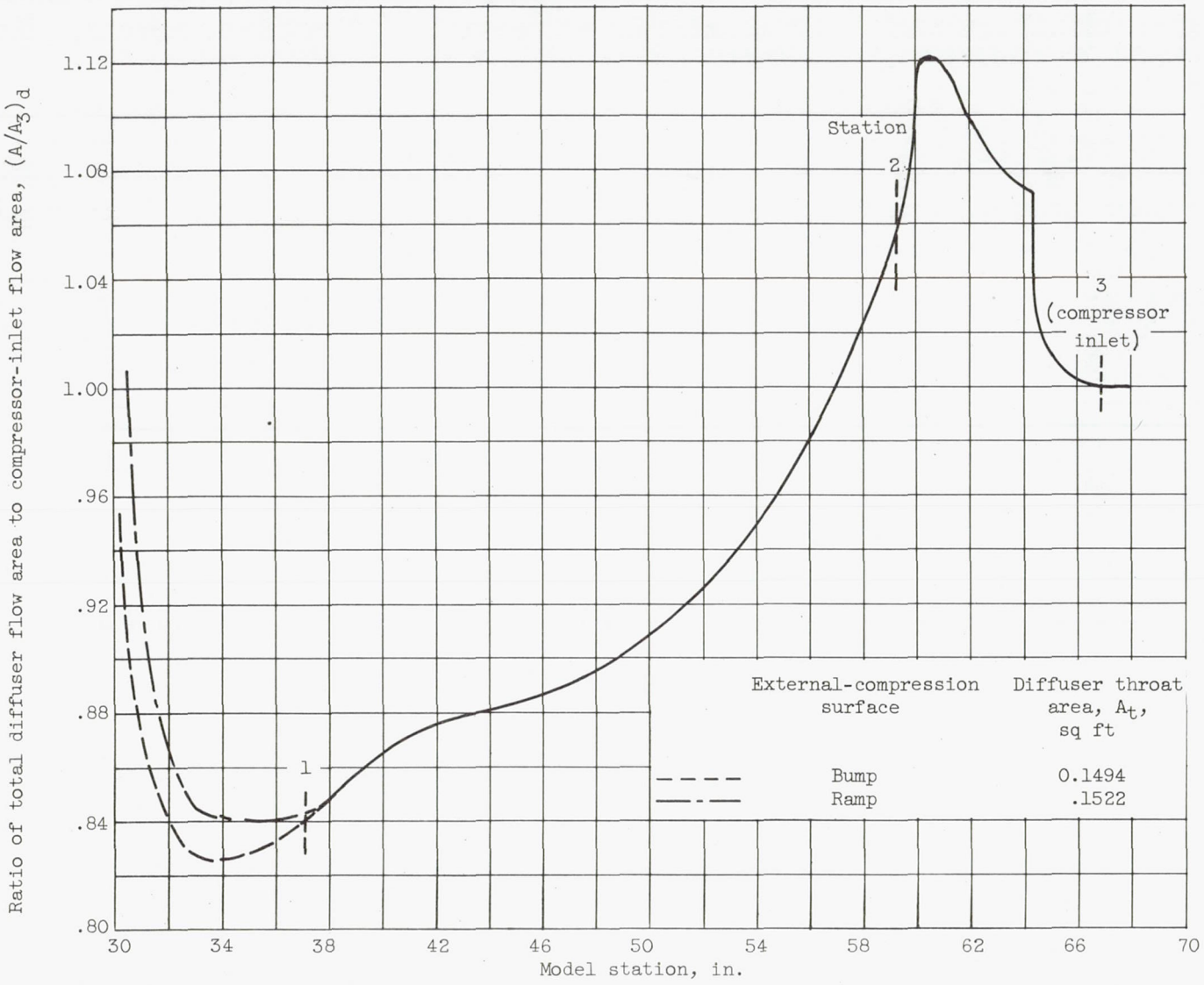
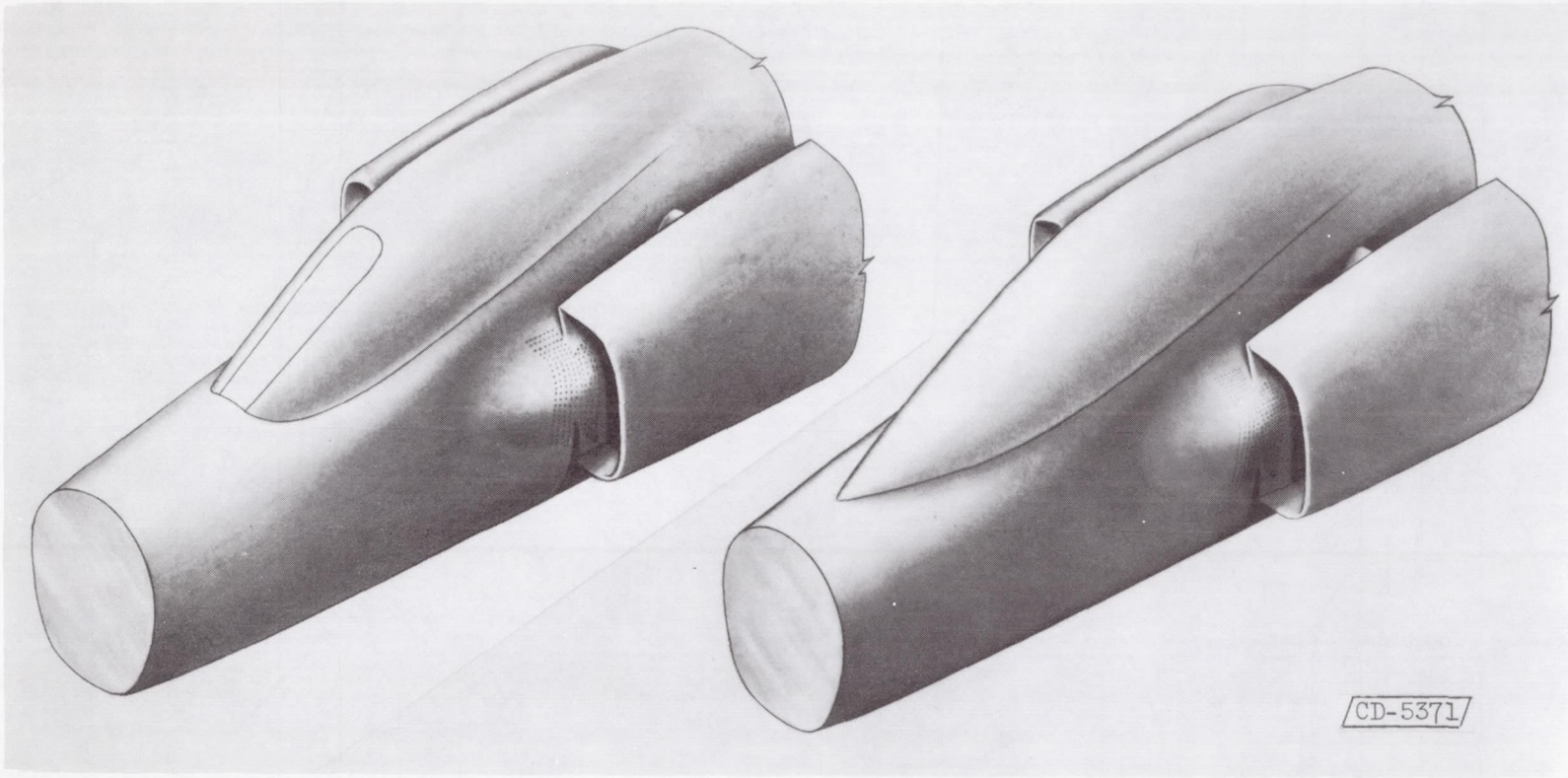


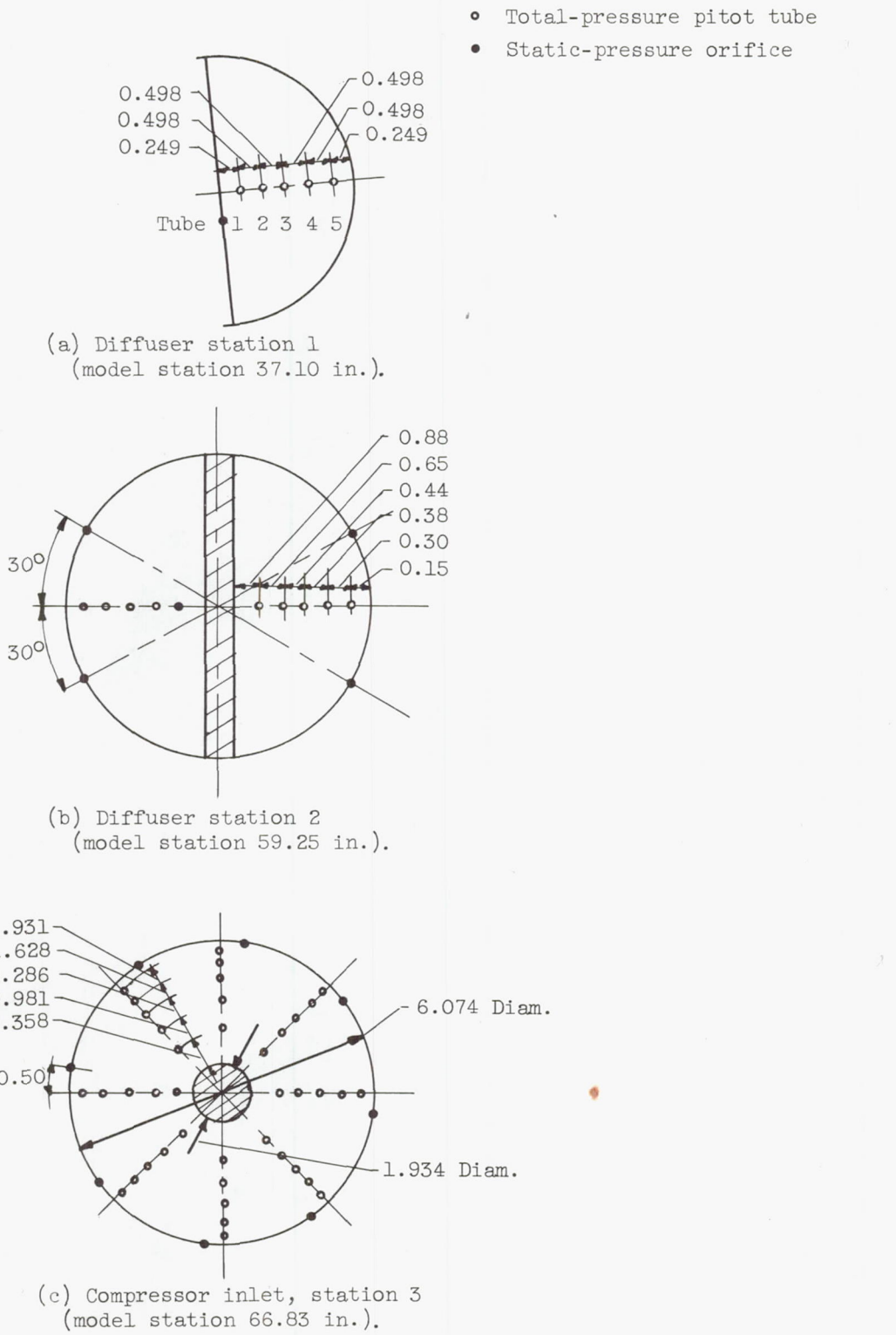
Figure 4. - Diffuser internal-flow-area variation. Compressor-inlet area, 0.1808 square foot.



(a) Flat windshield. (b) Conical windshield.

Figure 5. - Flat and conical canopies.

4350



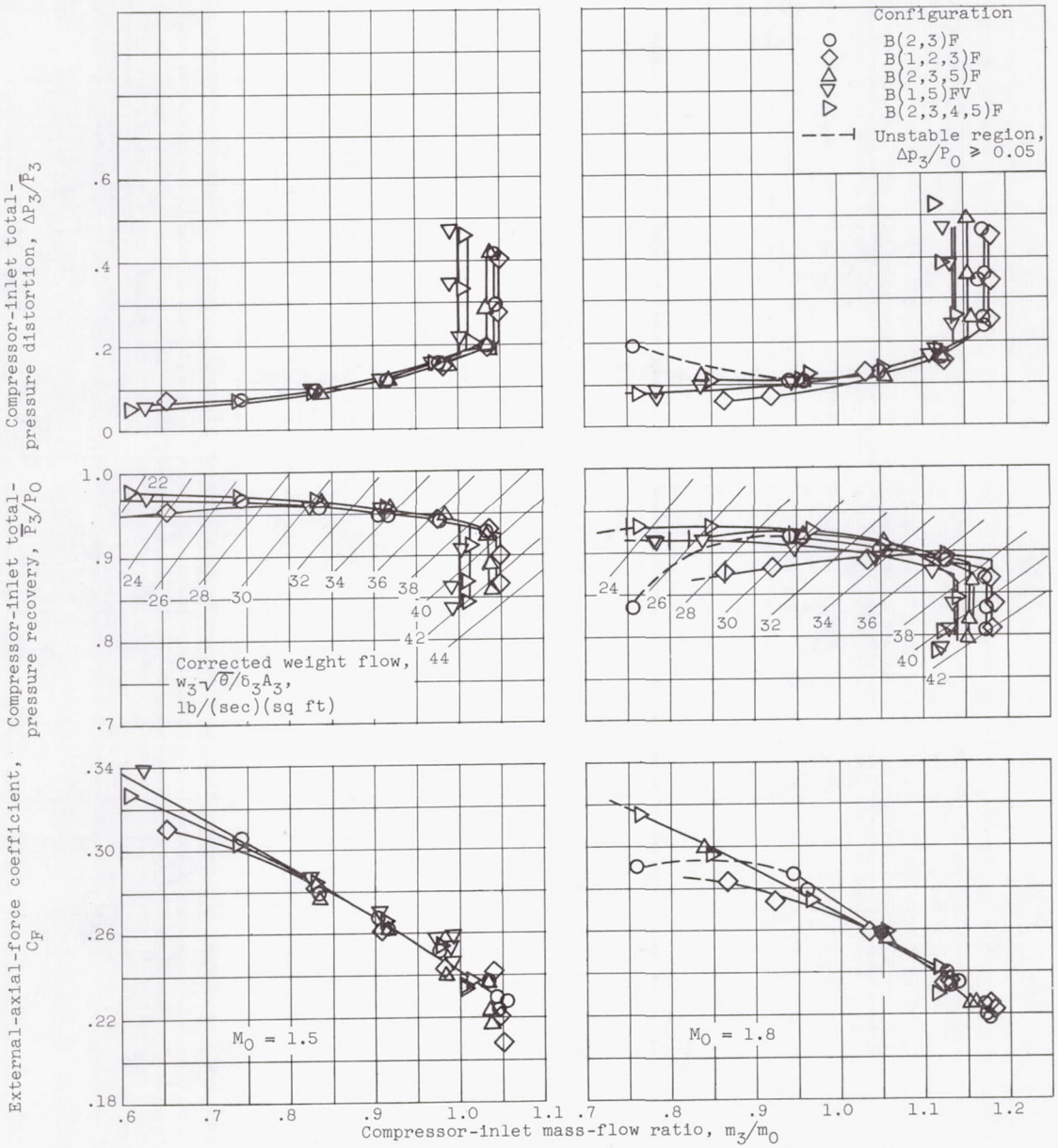
(a) Diffuser station 1 (model station 37.10 in.).

(b) Diffuser station 2 (model station 59.25 in.).

(c) Compressor inlet, station 3 (model station 66.83 in.).

Figure 6. - Schematic drawings of pressure-measuring instrumentation in diffuser. (All dimensions in inches.)

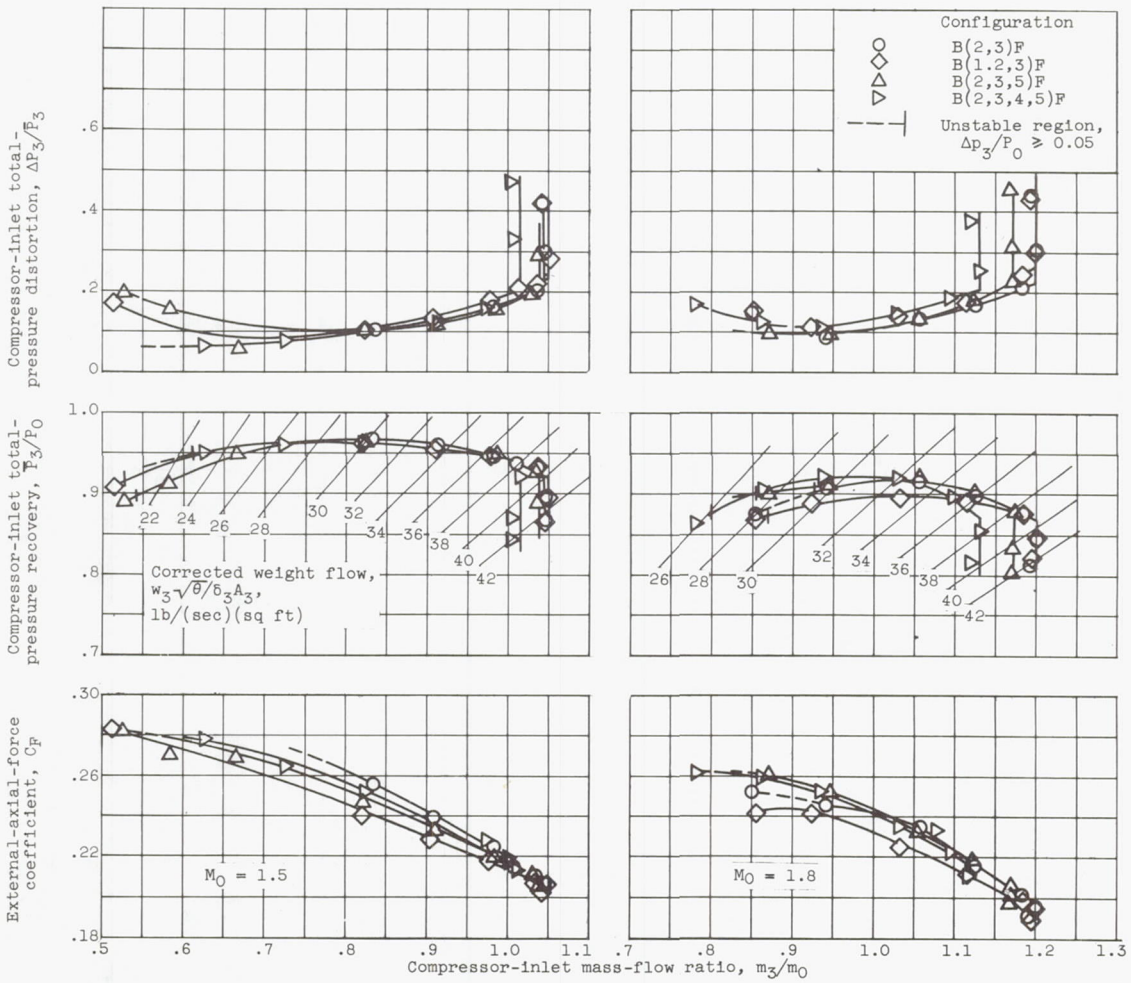
4350
CU-3 back



(a) Bump inlet with various bleed systems at zero angle of attack.

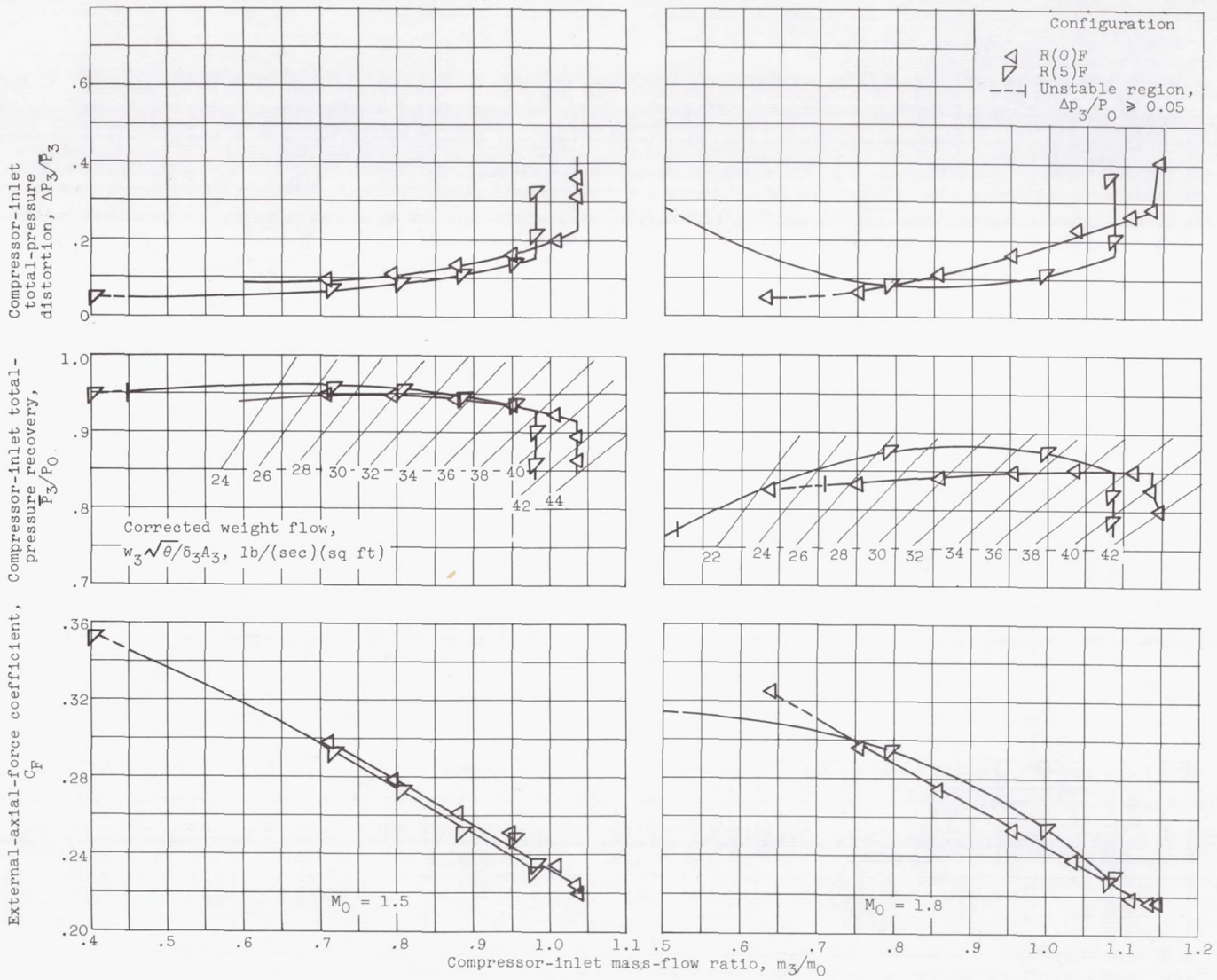
Figure 7. - Performance of configurations.

4350



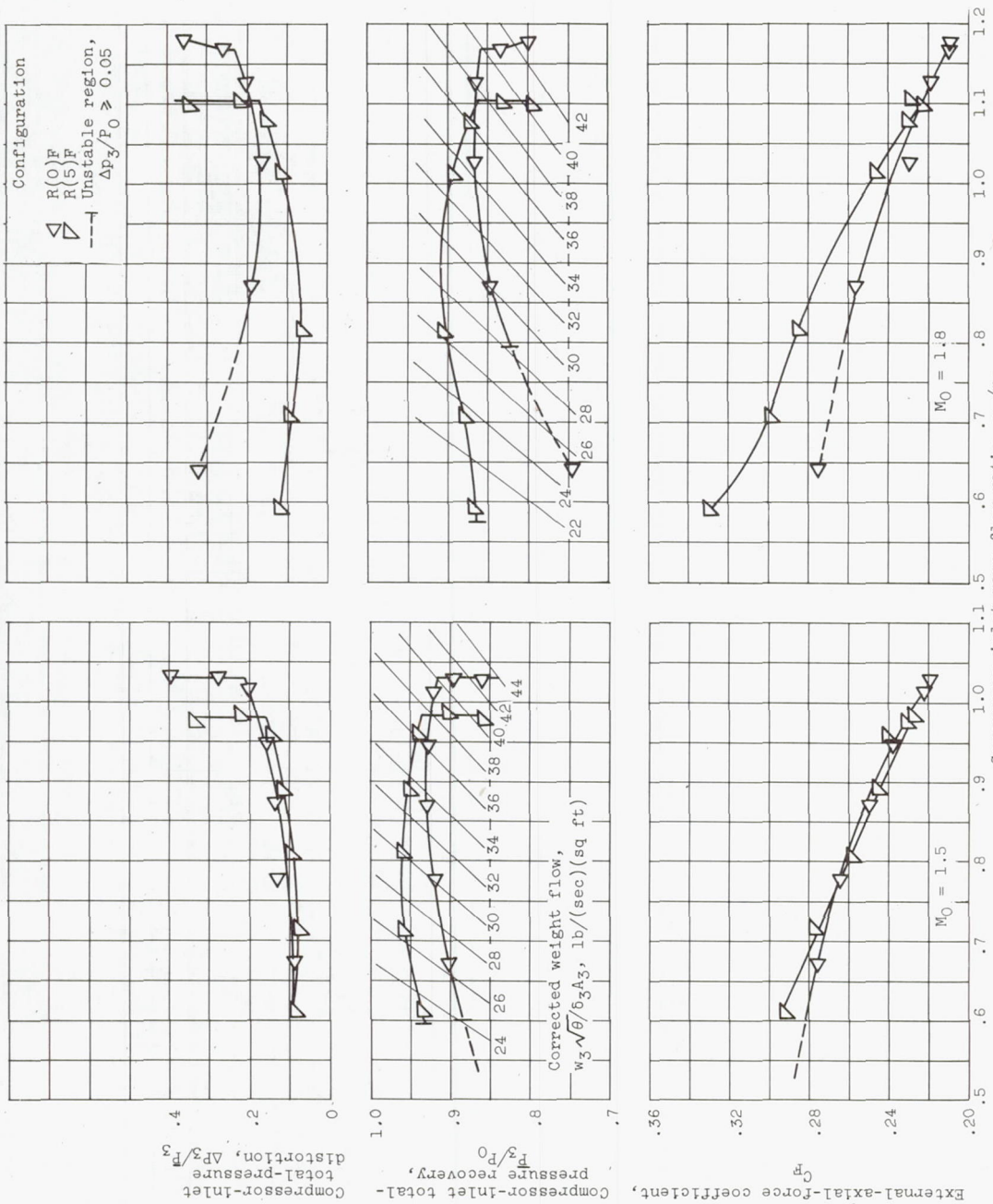
(b) Bump inlet with various bleed systems at 5° angle of attack.

Figure 7. - Continued. Performance of configurations.



(c) Ramp inlet with and without throat bleed at zero angle of attack.

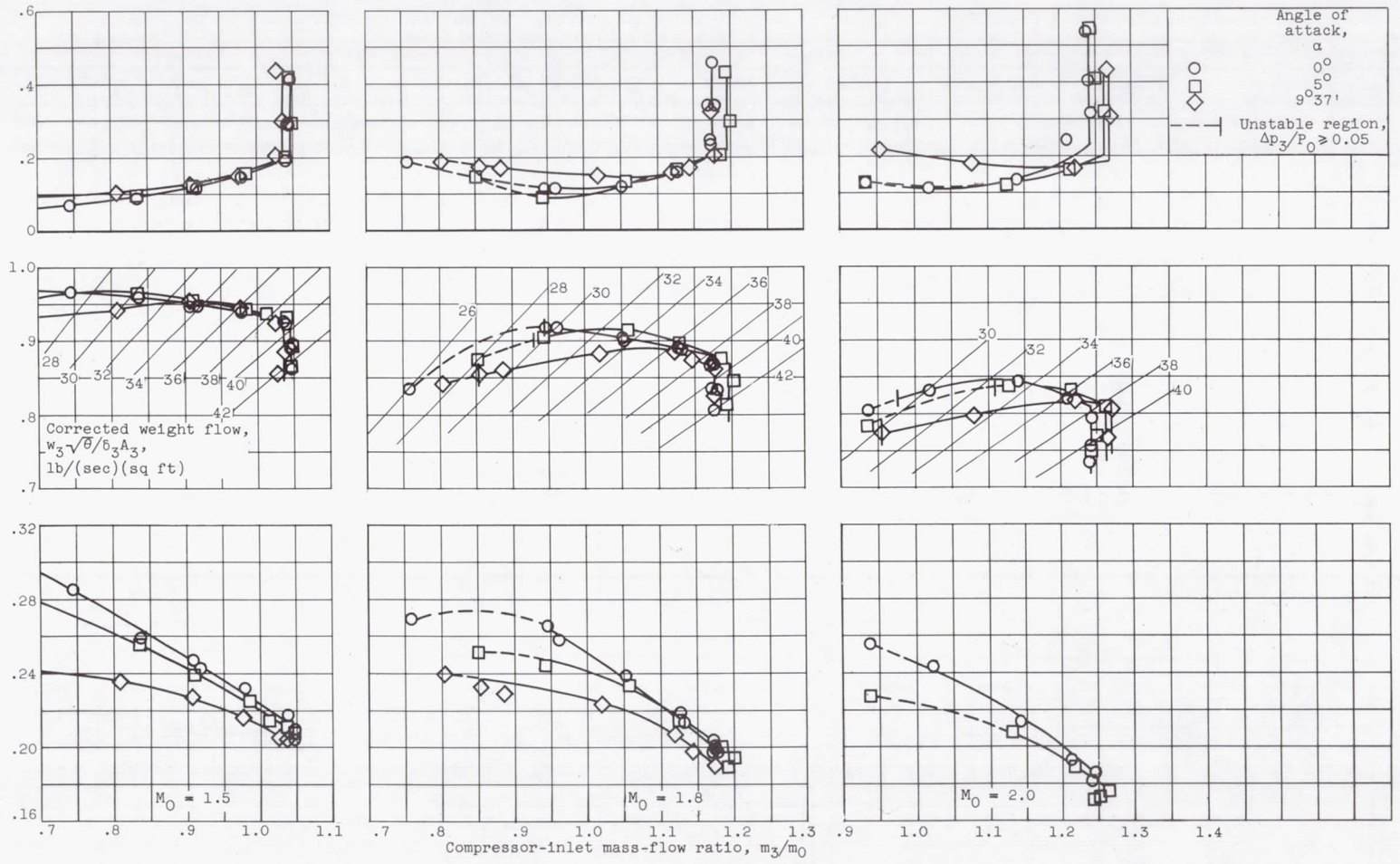
Figure 7. - Continued. Performance of configurations.



(d) Ramp inlet with and without throat bleed at 5° angle of attack.

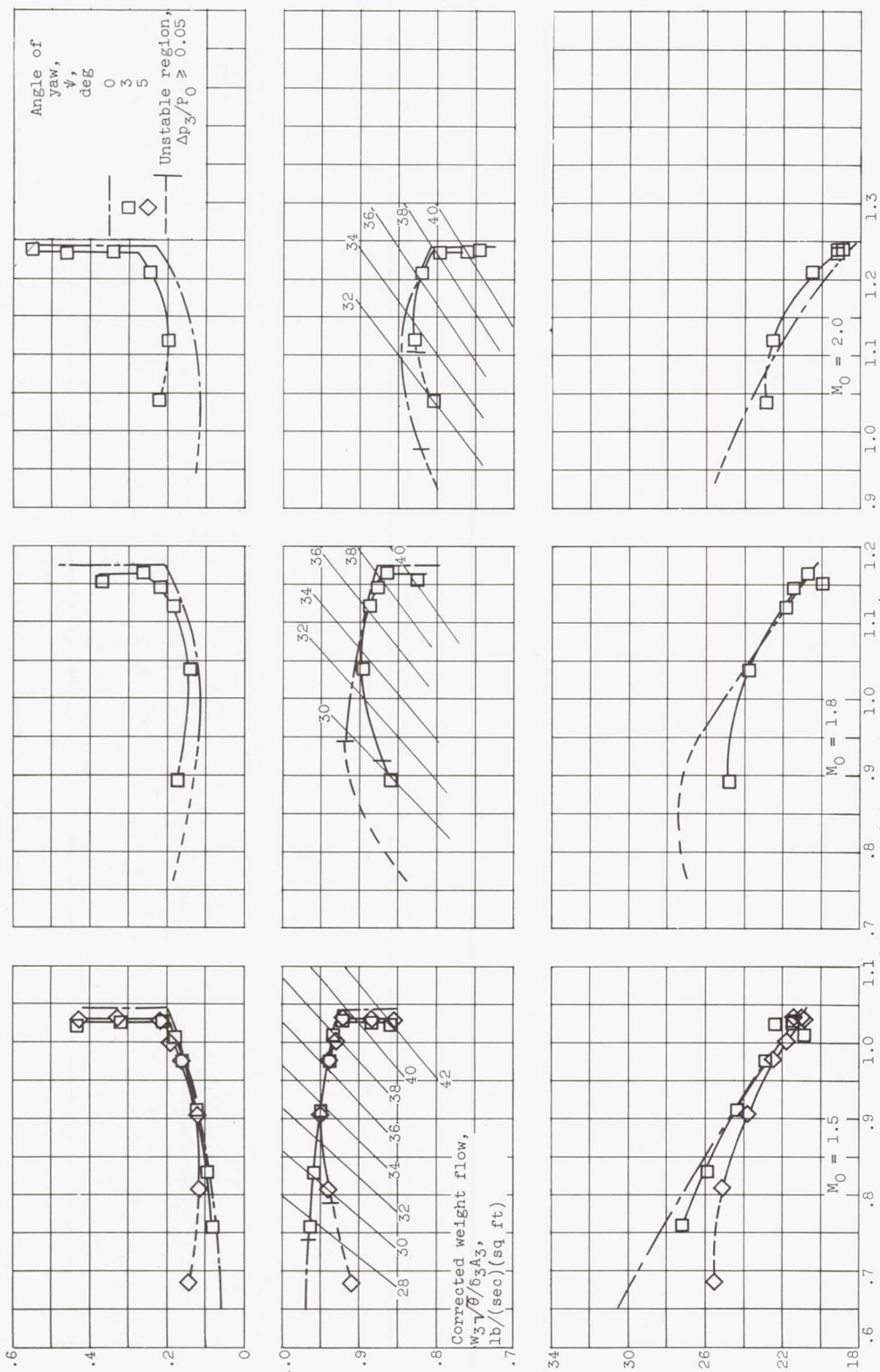
Figure 7. - Concluded. Performance of configurations.

4350



(a) Effect of angle of attack; configuration B(2,3)F.

Figure 8. - Performance of configuration B(2,3).

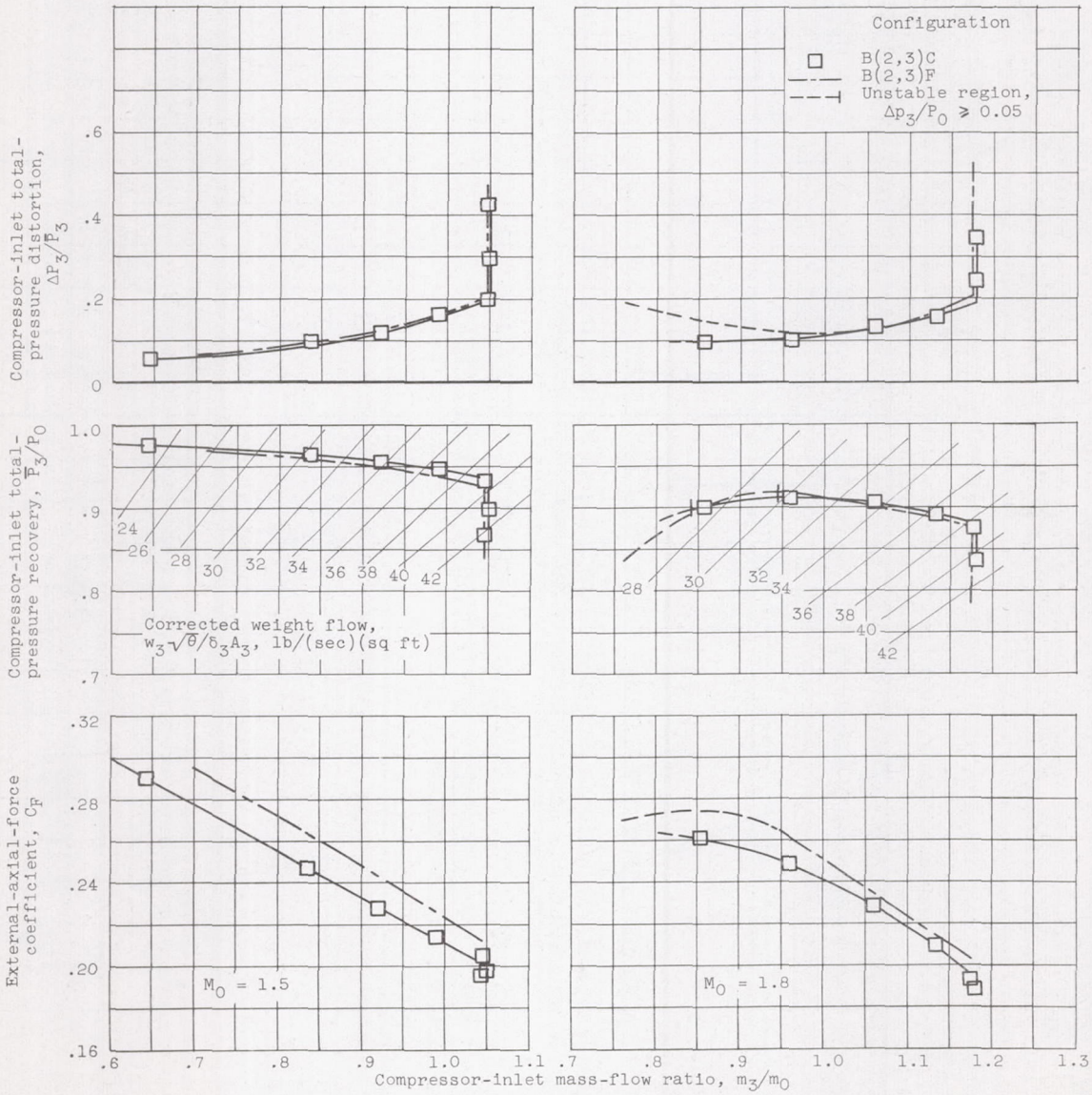


(b) Effect of angle of yaw; configuration B(2,3)F.

Figure 8. - Continued. Performance of configuration B(2,3).

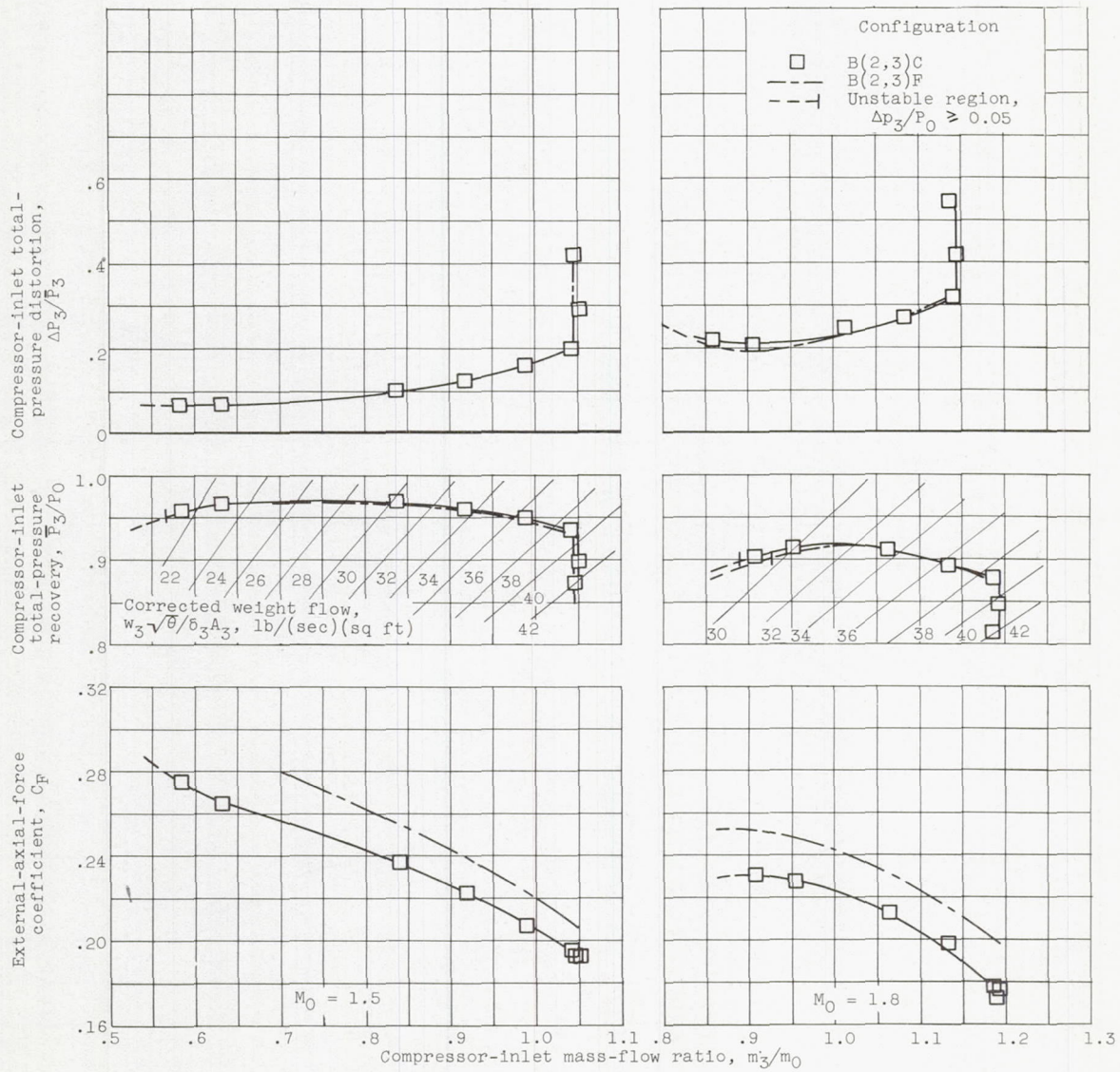
4350

4350 CU-4



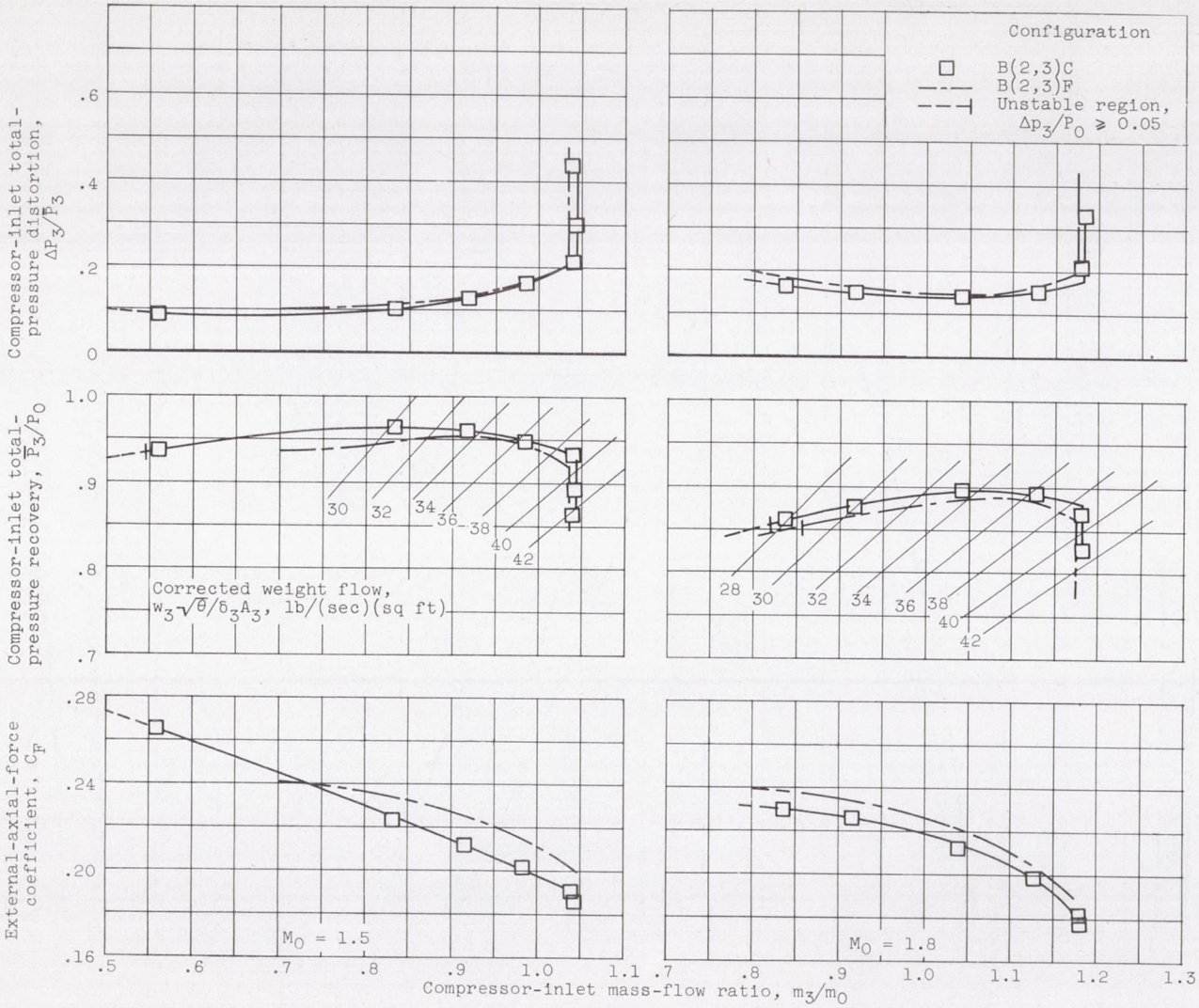
(c) Effect of canopy modification at zero angle of attack.

Figure 8. - Continued. Performance of configuration B(2,3).



(d) Effect of canopy modification at 5° angle of attack.

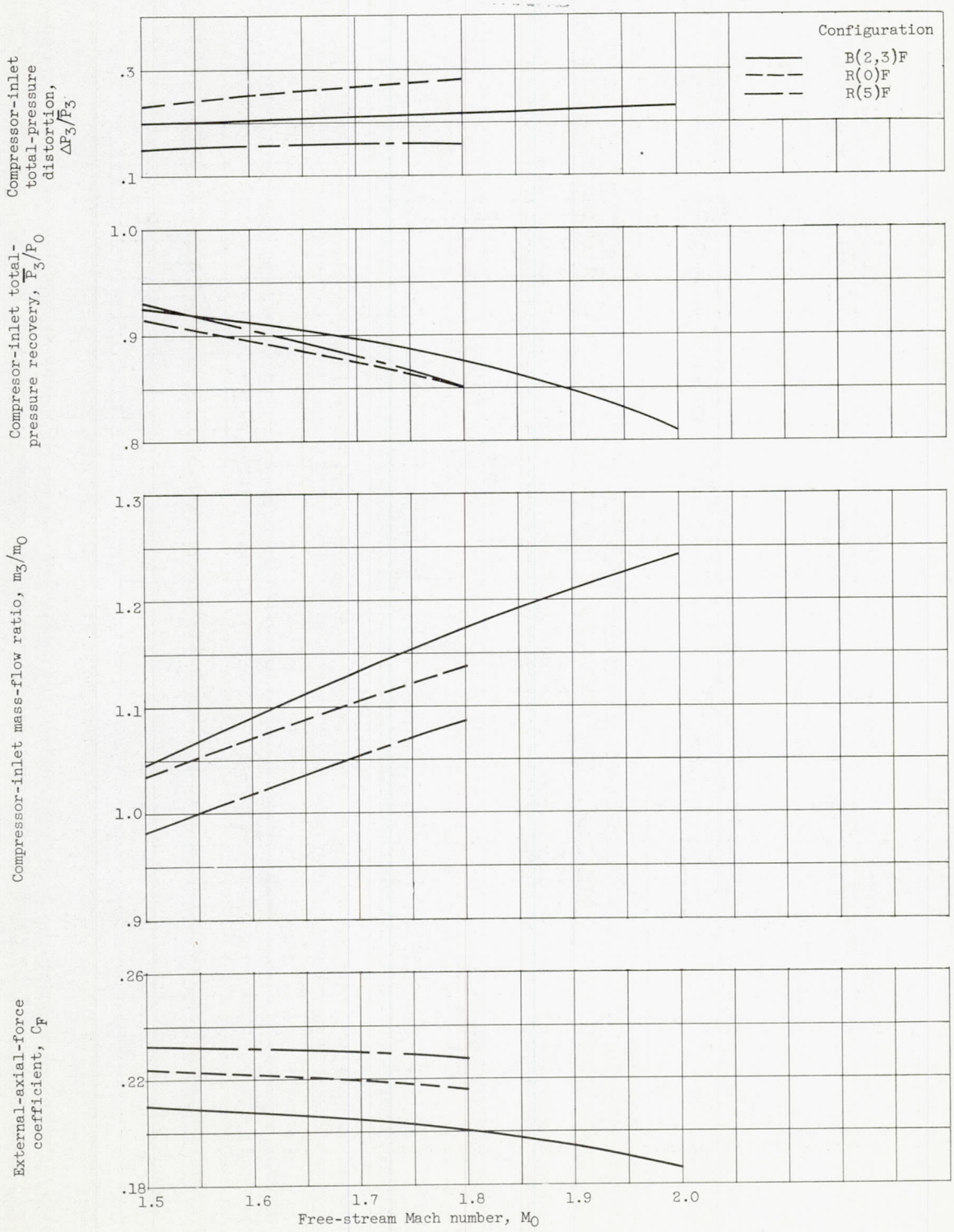
Figure 8. - Continued. Performance of configuration B(2,3).



(e) Effect of canopy modification at 9°37' angle of attack.

Figure 8. - Concluded. Performance of configuration B(2,3).

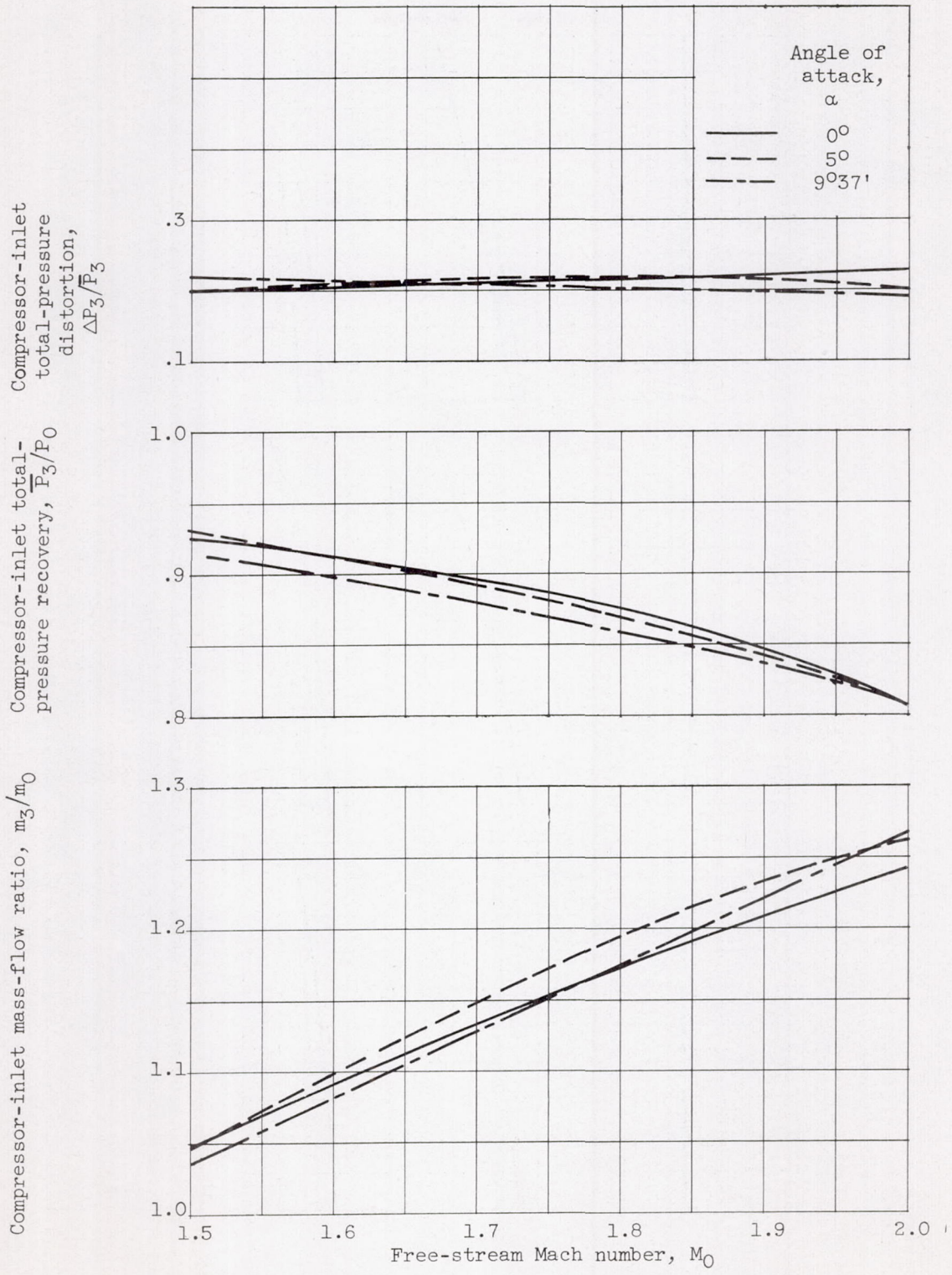
4350



(a) Three configurations at zero angle of attack.

Figure 9. - Summary of critical inlet performance.

4350

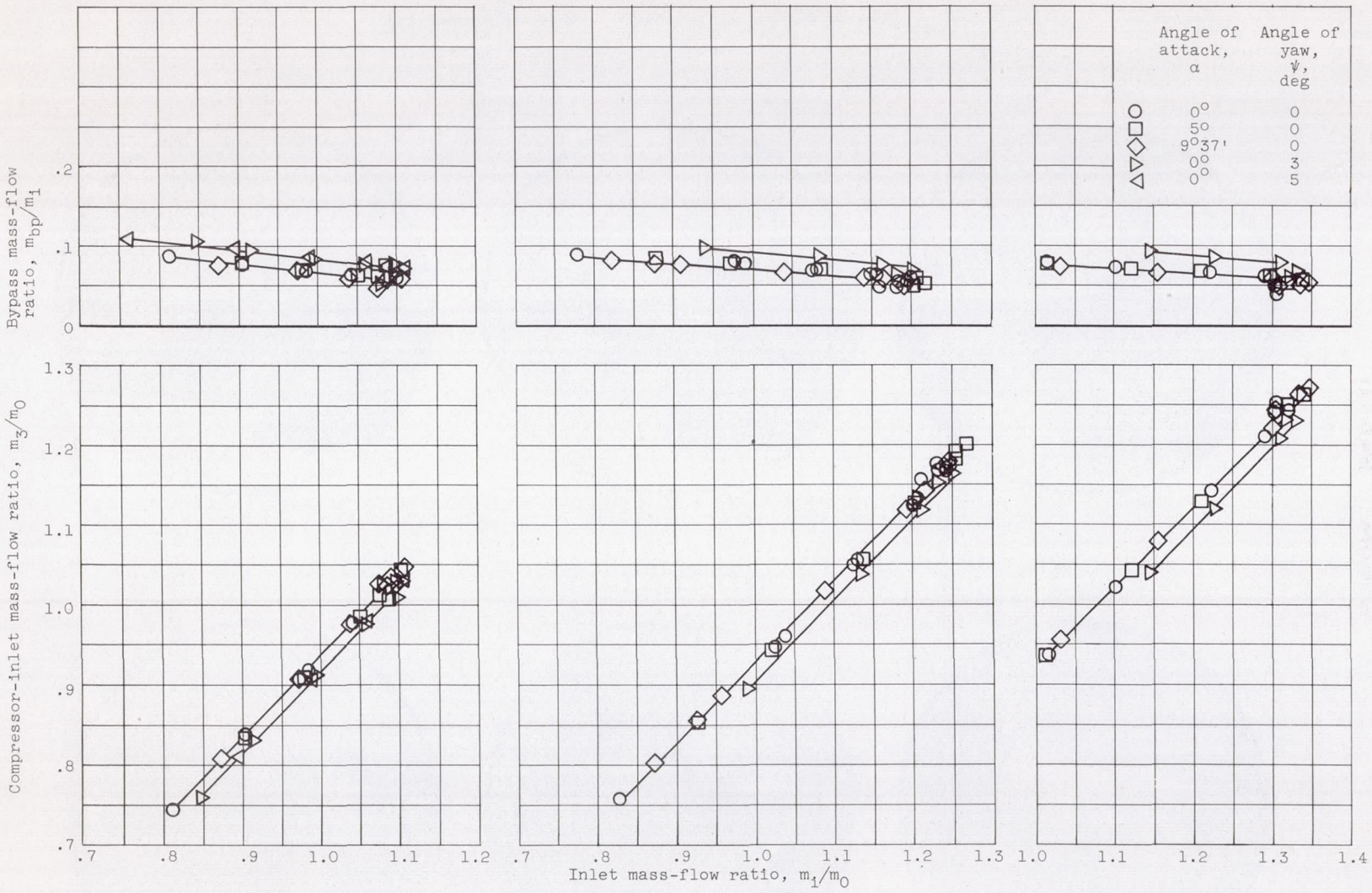


(b) Effect of angle of attack on configuration B(2,3)F.

Figure 9. - Continued. Summary of critical inlet performance.

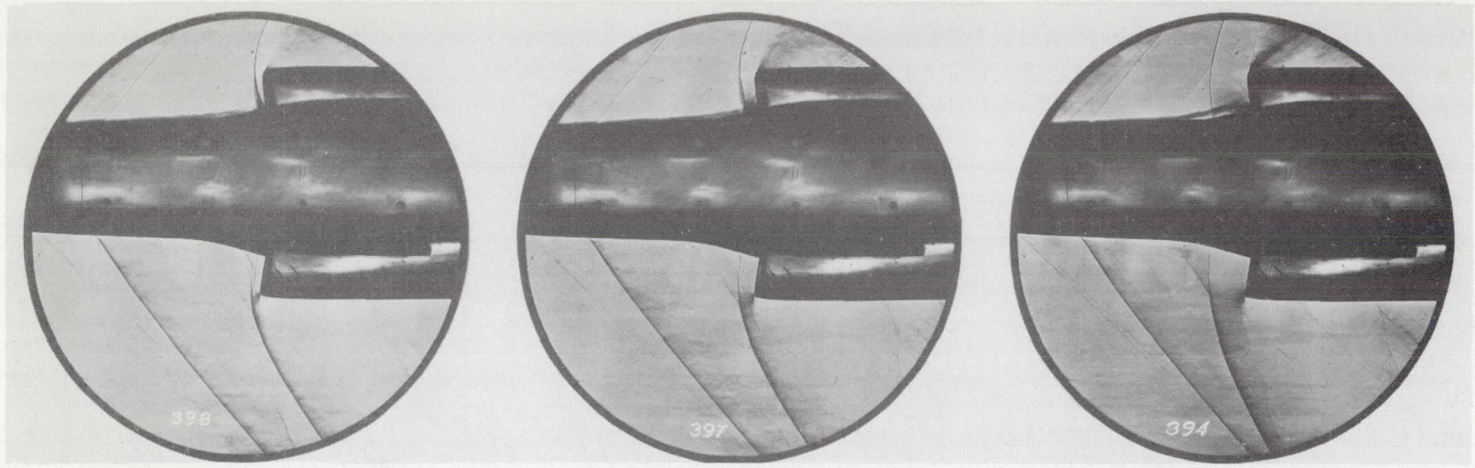
(c) Effect of canopy modification on configuration B(2,3) for angles of attack of 0°, 5°, and 9°37'.

Figure 9. - Concluded. Summary of critical inlet performance.



(a) Free-stream Mach number, 1.5. (b) Free-stream Mach number, 1.8. (c) Free-stream Mach number, 2.0.

Figure 10. - Compressor-inlet and bypass mass flow for configuration B(2,3)F.

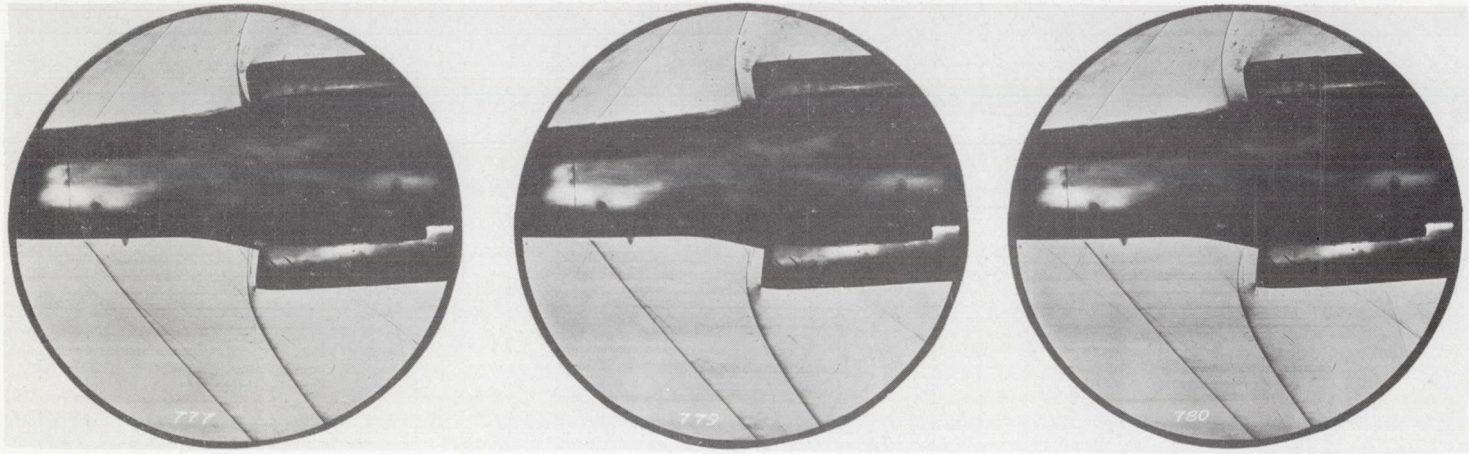


Critical
m_i/m_0 = 1.103

Subcritical
m_i/m_0 = 0.985

Subcritical
m_i/m_0 = 0.495

(a) Free-stream Mach number, 1.5; angle of yaw, 0°.



Critical
m_i/m_0 = 1.106

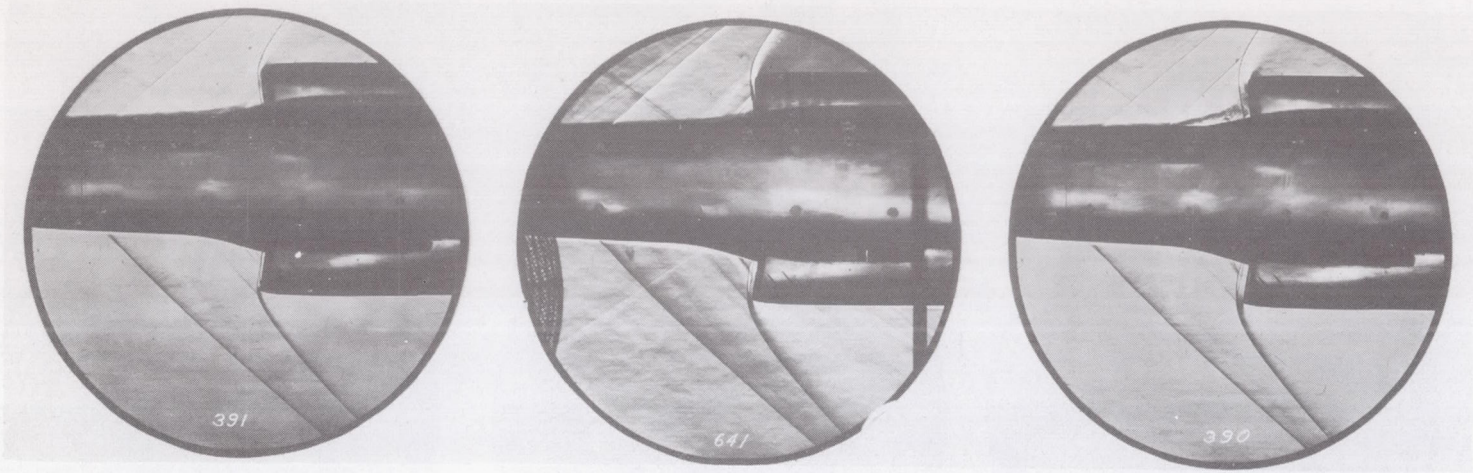
Subcritical
m_i/m_0 = 0.995

Subcritical
m_i/m_0 = 0.916

(b) Free-stream Mach number, 1.5; angle of yaw, 3°.

C-43666

Figure 11. - Schlieren photographs of configuration B(2,3)F at zero angle of attack.

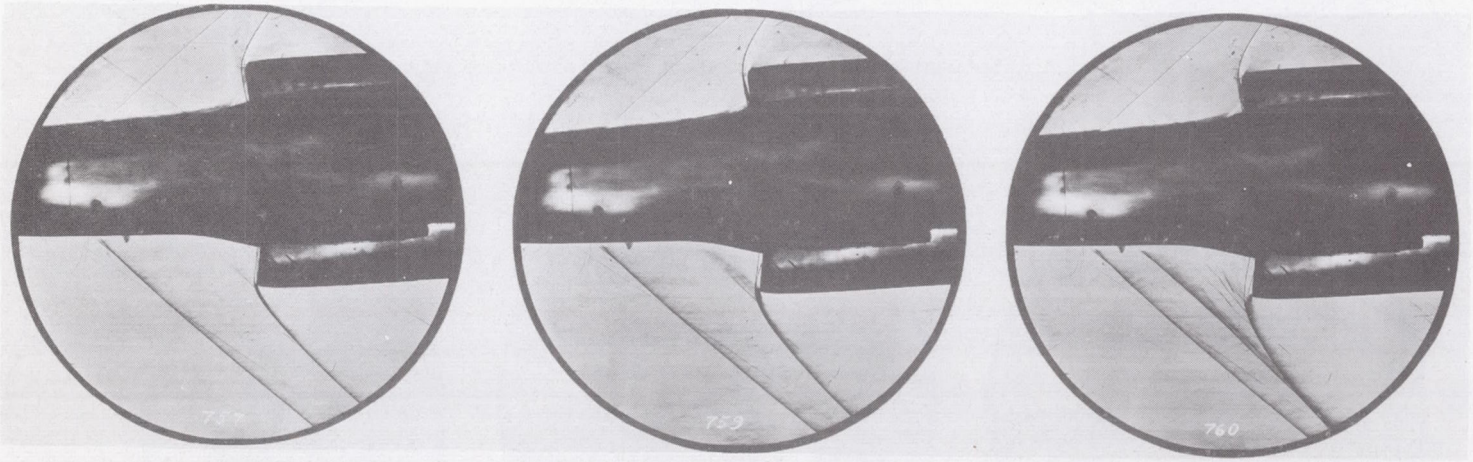


Critical
m_i/m_o = 1.241

Subcritical
m_i/m_o = 1.166

Subcritical
m_i/m_o = 1.069

(c) Free-stream Mach number, 1.8; angle of yaw, 0°.



Critical
m_i/m_o = 1.250

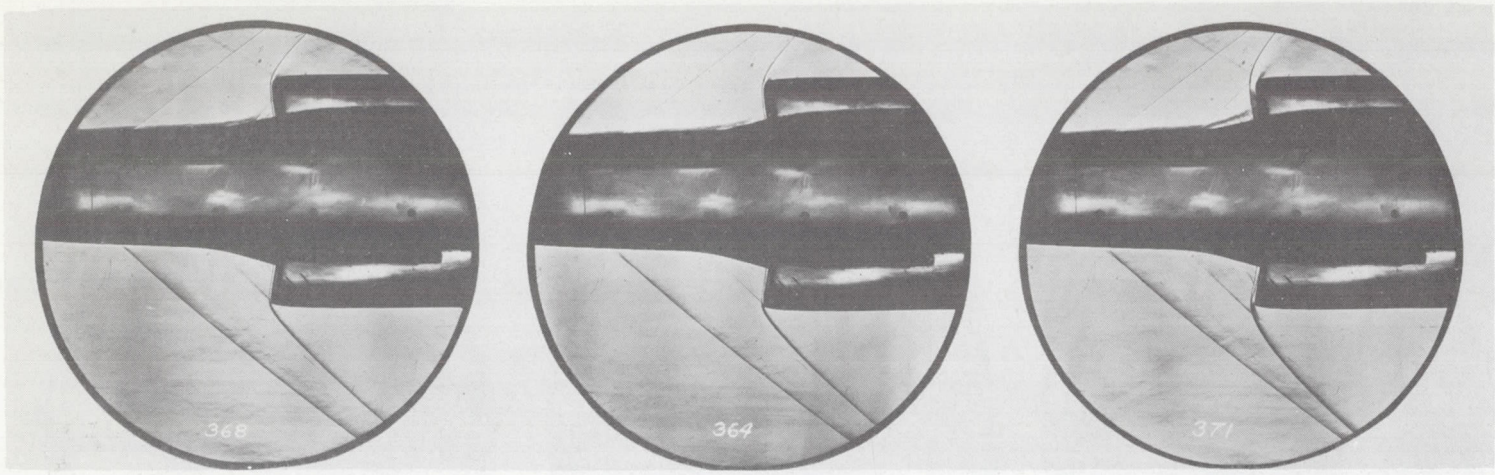
Subcritical
m_i/m_o = 1.134

Subcritical
m_i/m_o = 0.989

(d) Free-stream Mach number, 1.8; angle of yaw, 3°.

C-43667

Figure 11. - Continued. Schlieren photographs of configuration B(2,3)F at zero angle of attack.

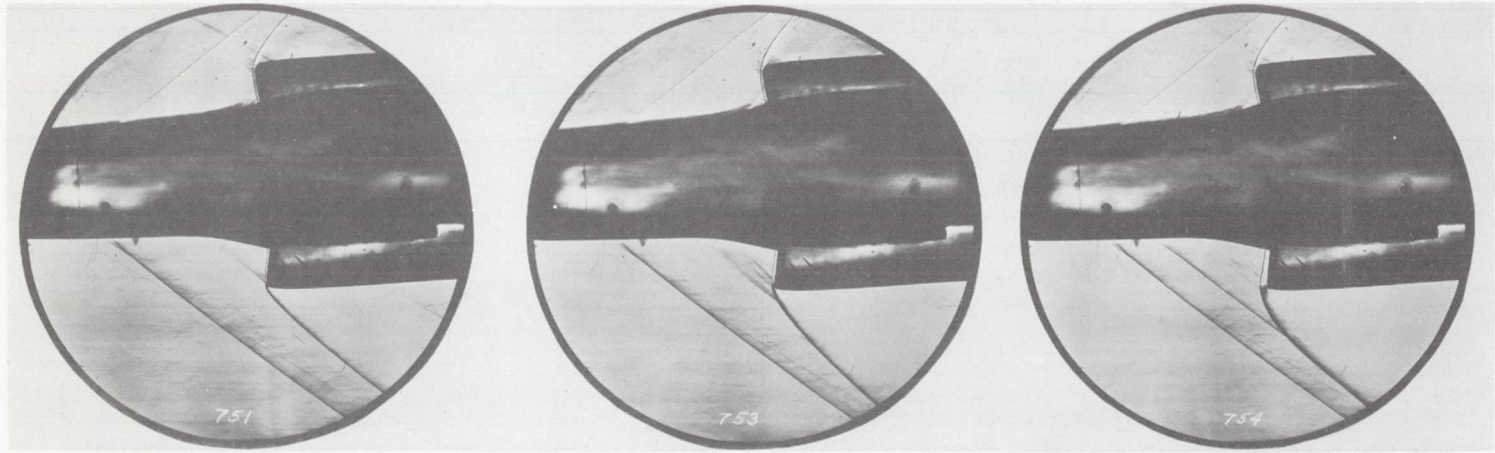


Critical
m_i/m_0 = 1.312

Subcritical
m_i/m_0 = 1.291

Subcritical
m_i/m_0 = 1.132

(e) Free-stream Mach number, 2.0; angle of yaw, 0°.



Critical
m_i/m_0 = 1.330

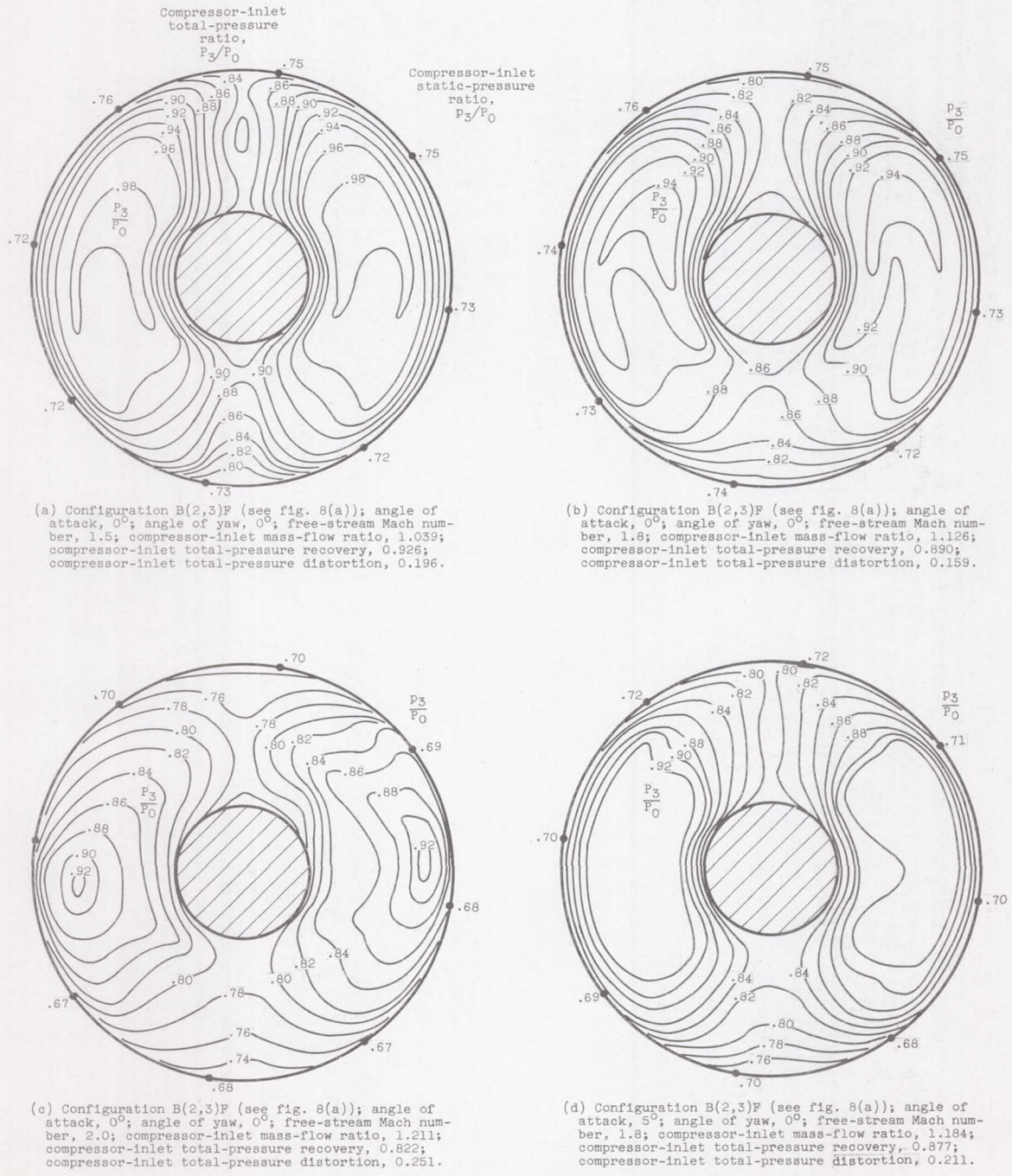
Subcritical
m_i/m_0 = 1.226

Subcritical
m_i/m_0 = 1.146

(f) Free-stream Mach number, 2.0; angle of yaw, 3°. C-43665

Figure 11. - Concluded. Schlieren photographs of configuration B(2,3)F at zero angle of attack.

4350
CU-5 back



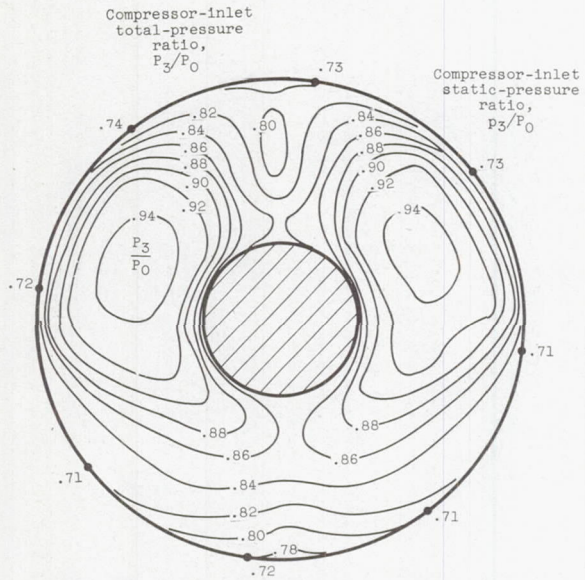
(a) Configuration B(2,3)F (see fig. 8(a)); angle of attack, 0°; angle of yaw, 0°; free-stream Mach number, 1.5; compressor-inlet mass-flow ratio, 1.039; compressor-inlet total-pressure recovery, 0.926; compressor-inlet total-pressure distortion, 0.196.

(b) Configuration B(2,3)F (see fig. 8(a)); angle of attack, 0°; angle of yaw, 0°; free-stream Mach number, 1.8; compressor-inlet mass-flow ratio, 1.126; compressor-inlet total-pressure recovery, 0.890; compressor-inlet total-pressure distortion, 0.159.

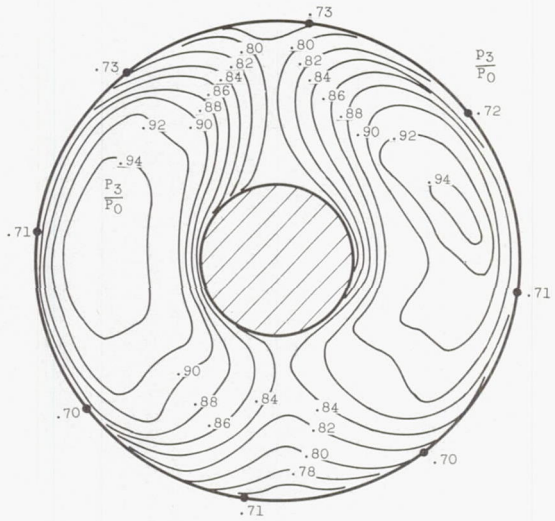
(c) Configuration B(2,3)F (see fig. 8(a)); angle of attack, 0°; angle of yaw, 0°; free-stream Mach number, 2.0; compressor-inlet mass-flow ratio, 1.211; compressor-inlet total-pressure recovery, 0.822; compressor-inlet total-pressure distortion, 0.251.

(d) Configuration B(2,3)F (see fig. 8(a)); angle of attack, 5°; angle of yaw, 0°; free-stream Mach number, 1.8; compressor-inlet mass-flow ratio, 1.184; compressor-inlet total-pressure recovery, 0.877; compressor-inlet total-pressure distortion, 0.211.

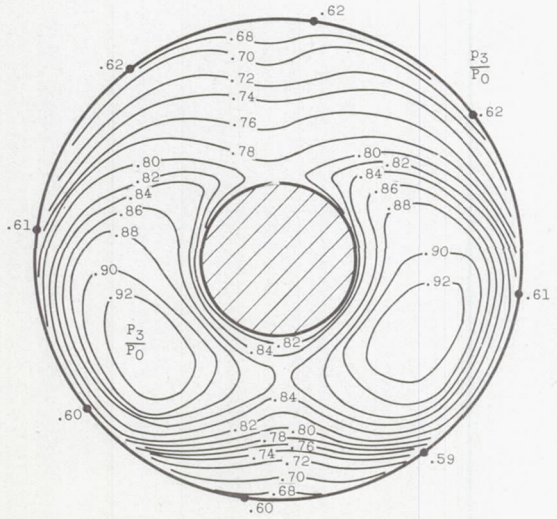
Figure 12. - Compressor-inlet total-pressure contours for several configurations (looking downstream).



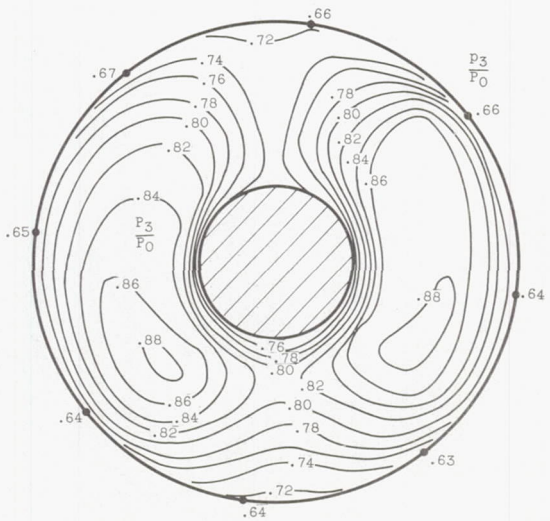
(e) Configuration B(2,3)F (see fig. 8(a)); angle of attack, 9°37'; angle of yaw, 0°; free-stream Mach number, 1.8; compressor-inlet mass-flow ratio, 1.145; compressor-inlet total-pressure recovery, 0.876; compressor-inlet total-pressure distortion, 0.179.



(f) Configuration B(2,3)F (see fig. 8(b)); angle of attack, 0°; angle of yaw, 3°; free-stream Mach number, 1.8; compressor-inlet mass-flow ratio, 1.145; compressor-inlet total-pressure recovery, 0.875; compressor-inlet total-pressure distortion, 0.225.



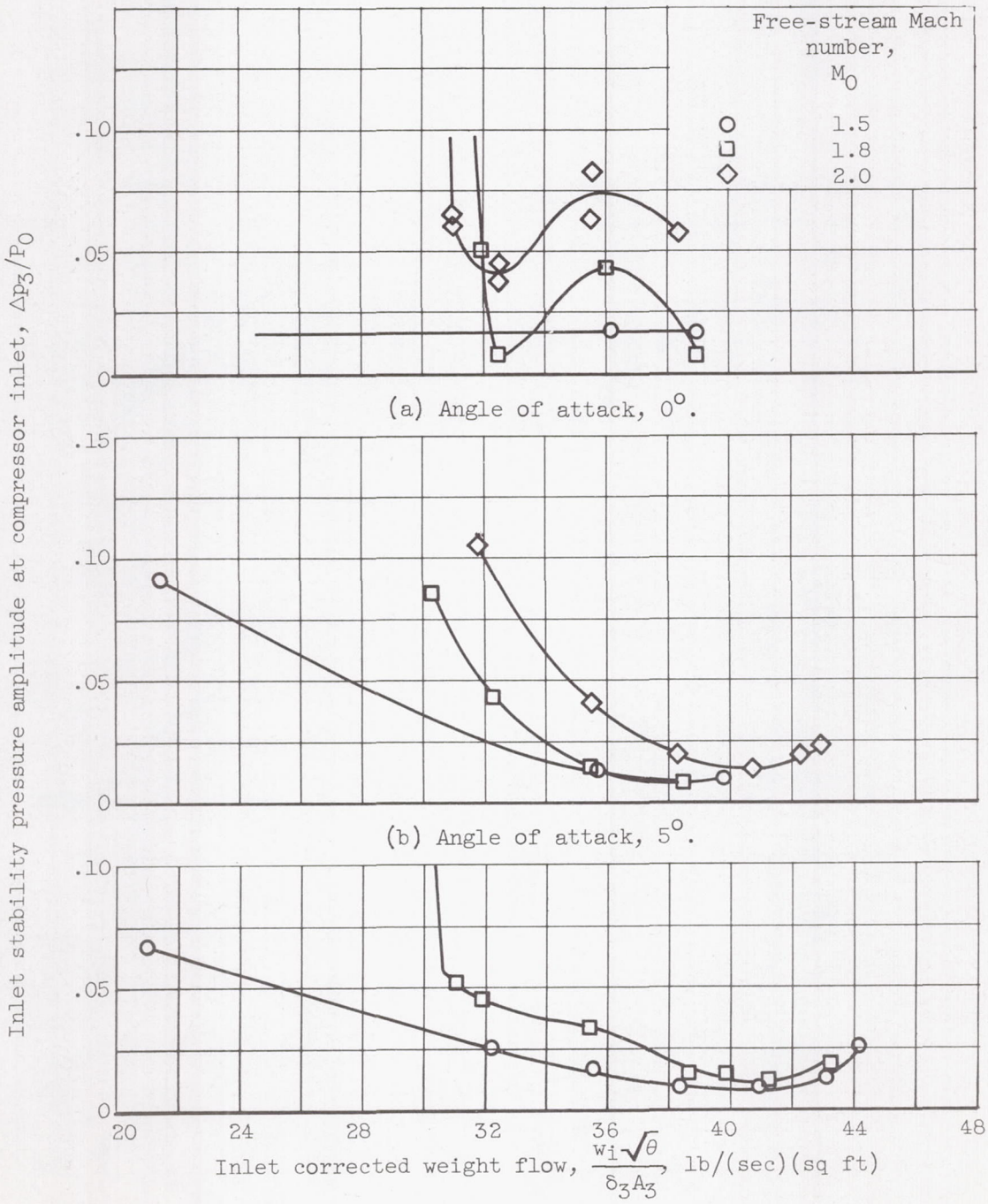
(g) Configuration R(0)F (see fig. 8(a)); angle of attack, 0°; angle of yaw, 0°; free-stream Mach number, 1.8; compressor-inlet mass-flow ratio, 1.137; compressor-inlet total-pressure recovery, 0.824; compressor-inlet total-pressure distortion, 0.283.



(h) Configuration R(5)F (see fig. 7(c)); angle of attack, 0°; angle of yaw, 0°; free-stream Mach number, 1.8; compressor-inlet mass-flow ratio, 1.088; compressor-inlet total-pressure recovery, 0.817; compressor-inlet total-pressure distortion, 0.197.

Figure 12. - Concluded. Compressor-inlet total-pressure contours for several configurations (looking downstream).

4350

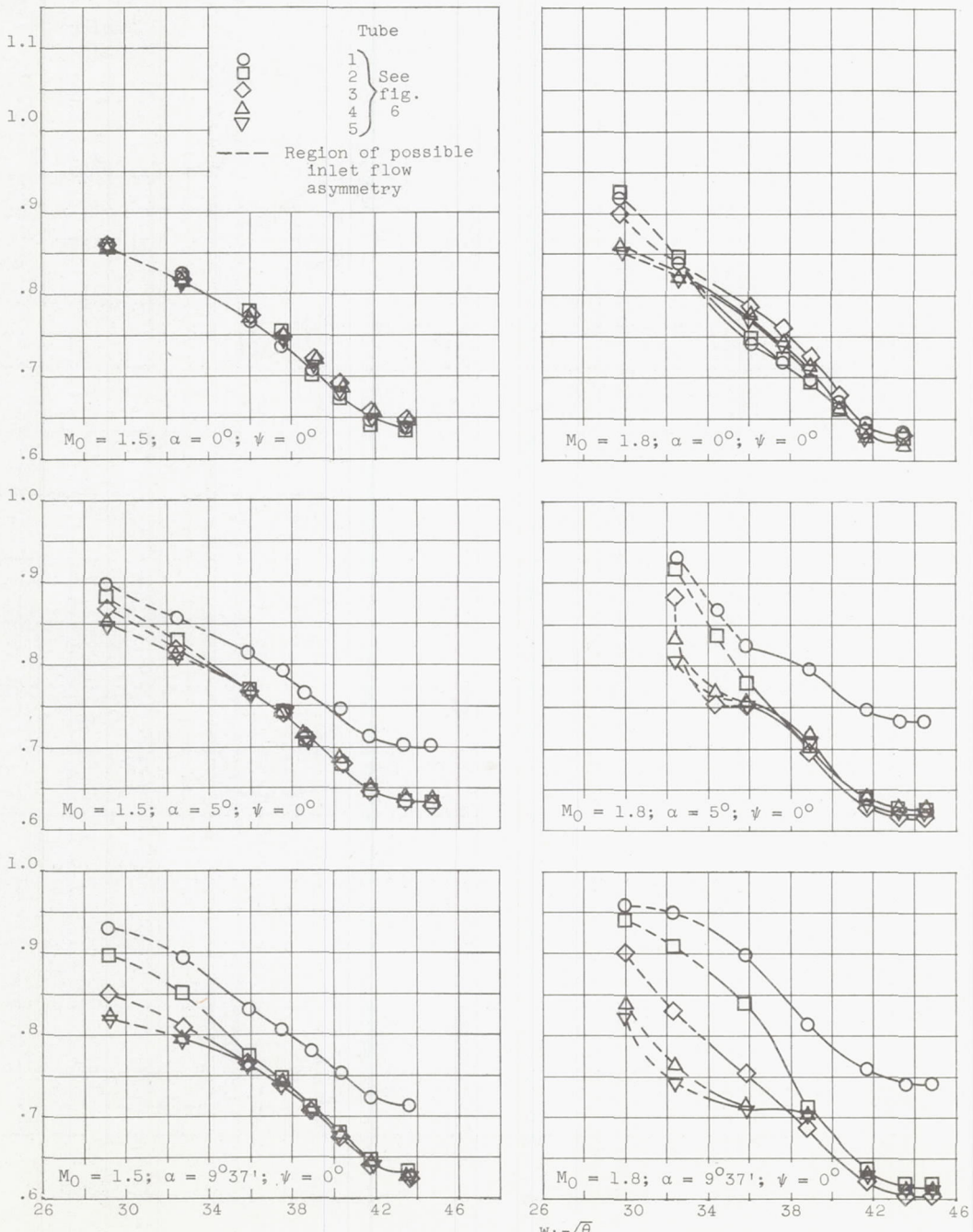


(a) Angle of attack, 0°.

(b) Angle of attack, 5°.

(c) Angle of attack, 9°37'.

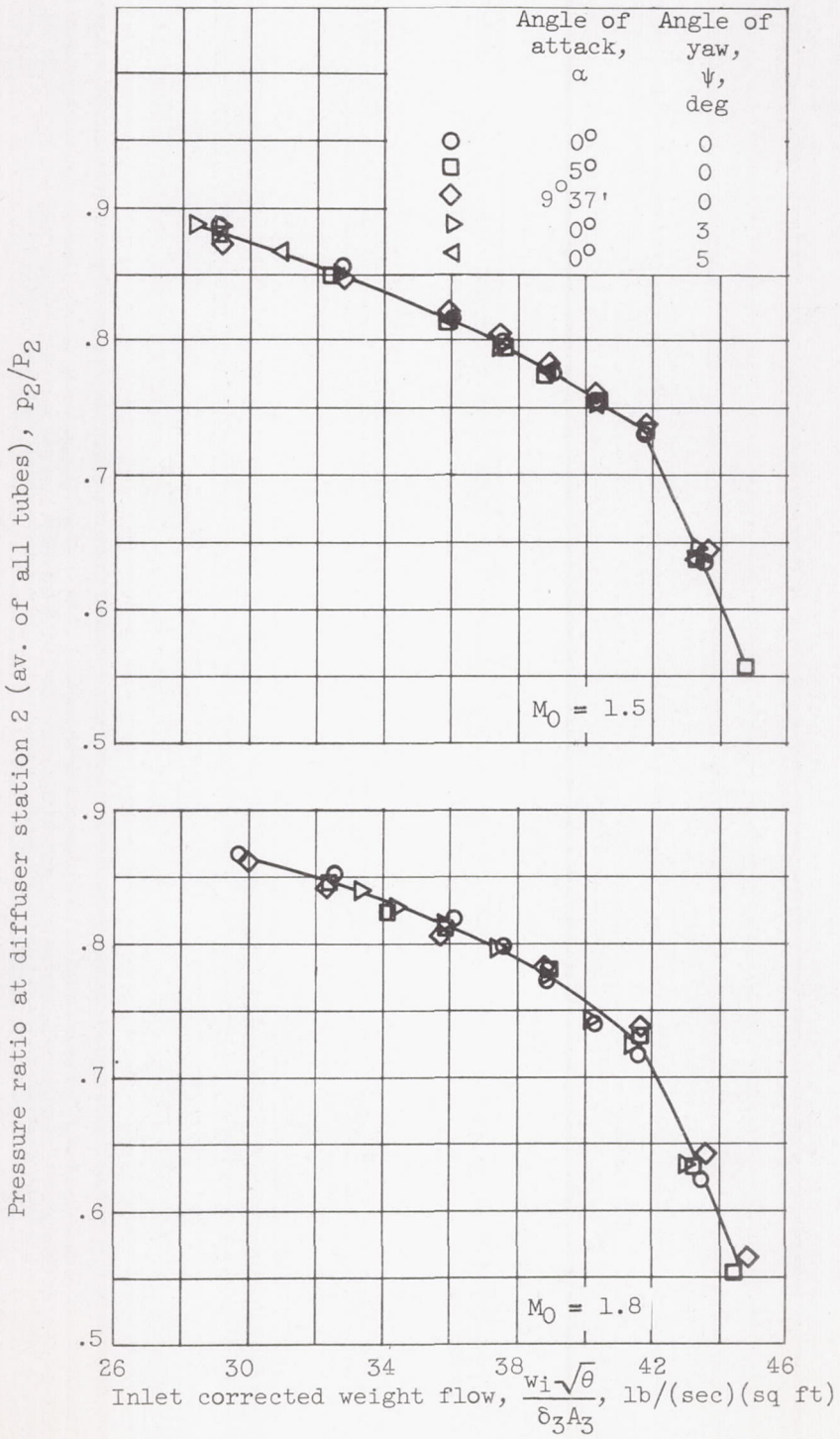
Figure 13. - Inlet stability in terms of static-pressure amplitude at compressor inlet for configuration B(2,3)F.



(a) Pressure ratio at diffuser station 1.

Figure 14. - Bypass control for configuration B(2,3)F.

4350



(b) Pressure ratio at diffuser station 2.

Figure 14 - Concluded. Bypass control for configuration B(2,3)F.

NACA - Langley Field, Va.